STAT3 gain-of-function mutations connect leukemia with autoimmune disease by pathological NKG2Dhi CD8+T cell dysregulation and accumulation

Masle-Farquhar, Etienne

2022-12-13

STAT3 gain-of-function mutations connect leukemia with autoimmune disease by pathological NKG2D^hi CD8+ T cell dysregulation and accumulation

Graphical abstract
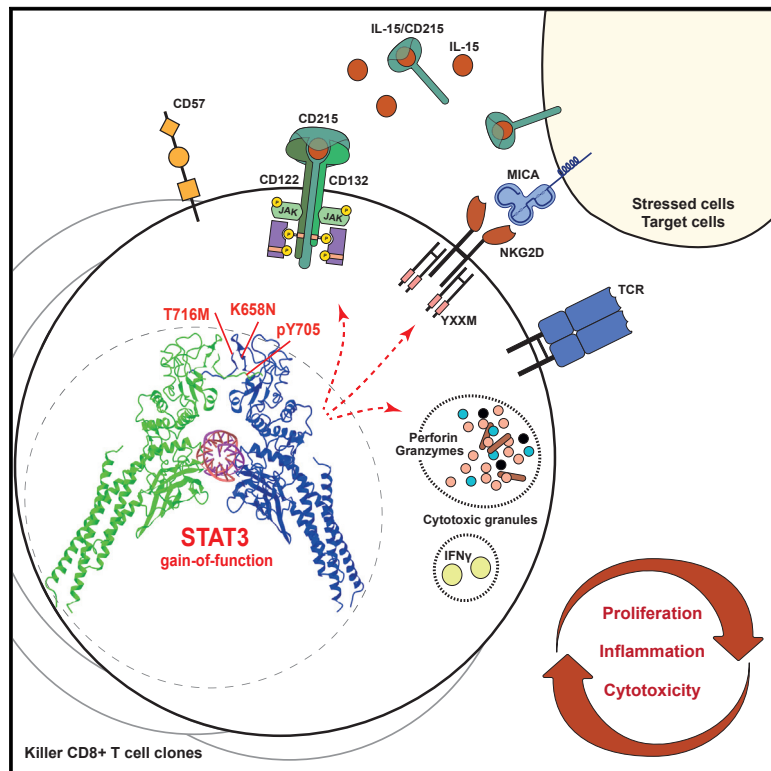
Authors

Etienne Masle-Farquhar,
Katherine J.L. Jackson,
Timothy J. Peters, ..., Stuart G. Tangye,
Joanne H. Reed,
Christopher C. Goodnow

Correspondence

e.masle-farquhar@garvan.org.au
(E.M.-F.),
c.goodnow@garvan.org.au (C.C.G.)

In brief

Whether somatic mutations are a cause or consequence of the autoimmune pathology associated with leukemia remains an unresolved issue. Here, Masle-Farquhar et al. show that leukemia and autoimmune-associated *STAT3* gain-of-function mutations dysregulate CD8+ T cells, driving oligoclonal expansion of cytotoxic CD8+ T cells and lethal inflammation.

Highlights

- Autoimmune-associated STAT3 GOF mutations pathologically dysregulate CD8 T cells

- STAT3 GOF somatic mutations in CD8 T cells are a cause, not effect, of autoimmunity

- STAT3 GOF mutant CD8 T cell accumulation depends on NKG2D and CD122/IL-15RB

- STAT3/NKG2D/IL-15 inhibitors may have utility in CD8-mediated autoimmune pathology

CellPress

Article

STAT3 gain-of-function mutations connect leukemia with autoimmune disease by pathological NKG2D^hi CD8+ T cell dysregulation and accumulation

Etienne Masle-Farquhar,[1,2,*] Katherine J.L. Jackson,[1] Timothy J. Peters,[1,2] Ghamdan Al-Eryani,[1,2] Mandeep Singh,[1,2] Kathryn J. Payne,[1] Geetha Rao,[1] Danielle T. Avery,[1] Gabrielle Apps,[1,3] Jennifer Kingham,[1,3] Christopher J. Jara,[1,2] Ksenia Skvortsova,[1,2] Alexander Swarbrick,[1,2] Cindy S. Ma,[1,2] Daniel Suan,[4] Gulbu Uzel,[5] Ignatius Chua,[6] Jennifer W. Leiding,[7,8] Kaarina Heiskanen,[9] Kahn Preece,[10] Leena Kainulainen,[11] Michael O'Sullivan,[12] Megan A. Cooper,[13] Mikko R.J. Seppänen,[14] Satu Mustjoki,[15,16,17] Shannon Brothers,[18] Tiphanie P. Vogel,[13] Robert Brink,[1,2] Stuart G. Tangye,[1,2] Joanne H. Reed,[1,2,20] and Christopher C. Goodnow[1,19,20,21,*]

[1]The Garvan Institute of Medical Research, Darlinghurst, Sydney, NSW 2010, Australia
[2]School of Clinical Medicine, UNSW Sydney, Sydney, NSW 2052, Australia
[3]Australian BioResources, Moss Vale, NSW 2577, Australia
[4]Westmead Clinical School, The University of Sydney, Westmead, Sydney, NSW, Australia
[5]Laboratory of Clinical Immunology and Microbiology, National Institute of Allergy and Infectious Diseases, NIH, Bethesda, MD, USA
[6]Canterbury Health Laboratories, Christchurch, New Zealand
[7]Division of Allergy and Immunology, Department of Pediatrics, University of South Florida, Tampa, FL, USA
[8]Division of Allergy and Immunology, Johns Hopkins All Children's Hospital, St. Petersburg, FL, USA
[9]Children's Immunodeficiency Unit, Hospital for Children and Adolescents, and Pediatric Research Center, Helsinki University Hospital and University of Helsinki, Helsinki, Finland
[10]Department of Immunology, John Hunter Children's Hospital, Newcastle, NSW, Australia
[11]Department of Pediatrics, Turku University Hospital, University of Turku, Turku, Finland
[12]Immunology Department, Fiona Stanley Hospital, Murdoch, WA, Australia
[13]Department of Pedatrics, Division of Rheumatology/Immunology, Washington University School of Medicine, St. Louis, MO, USA
[14]Rare Disease and Pediatric Research Centers, Hospital for Children and Adolescents, Helsinki University Hospital and University of Helsinki, Helsinki, Finland
[15]Hematology Research Unit Helsinki, University of Helsinki and Helsinki University Hospital Comprehensive Cancer Center, Helsinki, Finland
[16]Translational Immunology Research Program and Department of Clinical Chemistry and Hematology, University of Helsinki, Helsinki, Finland
[17]iCAN Digital Precision Cancer Medicine Flagship, Helsinki, Finland
[18]Starship Children's Hospital, Auckland, New Zealand
[19]Cellular Genomics Futures Institute, UNSW Sydney, Sydney, NSW, Australia
[20]These authors contributed equally
[21]Lead contact
*Correspondence: e.masle-farquhar@garvan.org.au (E.M.-F.), c.goodnow@garvan.org.au (C.C.G.)
https://doi.org/10.1016/j.immuni.2022.11.001

SUMMARY

The association between cancer and autoimmune disease is unexplained, exemplified by T cell large granular lymphocytic leukemia (T-LGL) where gain-of-function (GOF) somatic *STAT3* mutations correlate with co-existing autoimmunity. To investigate whether these mutations are the cause or consequence of CD8+ T cell clonal expansions and autoimmunity, we analyzed patients and mice with germline *STAT3* GOF mutations. STAT3 GOF mutations drove the accumulation of effector CD8+ T cell clones highly expressing NKG2D, the receptor for stress-induced MHC-class-I-related molecules. This subset also expressed genes for granzymes, perforin, interferon-γ, and *Ccl5*/Rantes and required NKG2D and the IL-15/IL-2 receptor IL2RB for maximal accumulation. Leukocyte-restricted *STAT3* GOF was sufficient and CD8+ T cells were essential for lethal pathology in mice. These results demonstrate that *STAT3* GOF mutations cause effector CD8+ T cell oligoclonal accumulation and that these rogue cells contribute to autoimmune pathology, supporting the hypothesis that somatic mutations in leukemia/lymphoma driver genes contribute to autoimmune disease.

INTRODUCTION

The pathogenesis of autoimmune diseases is incompletely understood. One hypothesis is that these diverse diseases share molecular roots with lymphoid cancer, wherein self-tissues are damaged by rogue lymphocyte clones that bypass tolerance checkpoints by acquiring somatic cancer driver gene mutations (Goodnow, 2007; Burnet, 1965).

CellPress
OPEN ACCESS

A

— Germline mutations in MGRB (1143 individuals)
— Germline mutations in STAT3 GOF syndrome (63 individuals)
— Somatic mutations in T-LGL (790 individuals). Mutation hotspots.
★ Mouse models included in this study

B

	WT	HET	HOM
Expected	25%	50%	25%
Stat3^T716M	144/424 34%	228/424 54%	52/424 12%
Stat3^K658N	47/138 34%	78/138 57%	13/138 9%

C

n=268 ○ Stat3^+/+
n=407 ○ Stat3^T716M/+
n=152 ○ Stat3^T716M/T716M
n=280 □ Stat3^+/+
n=434 □ Stat3^K658N/+
n=121 ■ Stat3^K658N/K658N

D

Stat3^+/+ (grey square)
Stat3^K658N/+ (orange square)
Stat3^K658N/K658N (red square)

Stat3^+/+ (grey circle)
Stat3^T716M/+ (light blue circle)
Stat3^T716M/T716M (blue circle)

E

Stat3^K658N	# of mice assessed	# with pathology
WT	171	3/171 (1.75%)
HET	40	29/40 (72.5%)
HOM	41	41/41 (100%)

F

n=14 □ Stat3^+/+
n=88 □ Stat3^K658N/+
n=33 ■ Stat3^K658N/K658N
n=11 □ Stat3^K658N/K658N Rag1^KO/+
n=13 ■ Stat3^K658N/K658N Rag1^KO/KO

G

Stat3^+/+   Stat3^K658N/K658N

H

Stat3^+/+ (grey circle) Stat3^T716M/+ (light blue circle) Stat3^T716M/T716M (blue circle)

Stat3^+/+ (grey square) Stat3^K658N/+ (orange square) Stat3^K658N/K658N (red square)

(legend on next page)

T cell large granular lymphocytic leukemia (T-LGL) is a striking, unexplained example of the intersection between lymphoproliferative disease and autoimmunity (Lamy et al., 2017; Zhang et al., 2010). CD8+ T-LGL is an indolent disorder defined by exuberant accumulation in blood of one or more expanded clones of large granular CD8+ T cells of phenotype CD28− CD27− CD45RA+ CD45RO− CD57+ perforin+ granzyme-b+. T-LGL is often diagnosed because of pathological neutrophil or erythrocyte deficiency presumed to reflect autoimmune destruction. T-LGL is frequently accompanied by rheumatoid arthritis (RA) and other autoimmune diseases (Lamy et al., 2017; Zhang et al., 2010). 50% of T-LGL patients harbor expanded CD8+ T cell clones bearing a gain-of-function (GOF) somatic mutation in *signal transducer and activator of transcription 3* (*STAT3*), and these patients more frequently have RA (Koskela et al., 2012). Although the population frequency for RA is <1%, of the 8% of T-LGL patients having multiple independent *STAT3*-mutant CD8+ clones, 43% have RA (Rajala et al., 2015). This correlation could be an effect of inflammation such as greater T cell proliferation increasing somatic mutations. Alternatively, *STAT3* GOF mutations in CD8+ T cells may cause autoimmune pathology.

Phosphorylated STAT3 activates gene transcription in response to myriad cytokines (Deenick et al., 2018; O'Shea et al., 2013). Memory CD8+ T cell persistence and function depend on STAT3, based on loss-of-function *STAT3* mutations in humans (Ives et al., 2013; Siegel et al., 2011) and mice (Cui et al., 2011). T-LGL *STAT3* mutations are overwhelmingly missense, clustering at the dimerization interface of the *Src* homology 2 (SH2) domain, creating GOF by increasing hydrophobicity and dimerization (Andersson et al., 2016; Barila et al., 2019; Fasan et al., 2013; Ishida et al., 2014; Jerez et al., 2012, 2013; Kerr et al., 2019; Koskela et al., 2012; Morgan et al., 2017; Qiu et al., 2013; Shi et al., 2018; de Araujo et al., 2019). Many of the mutations are in small clones representing <5% of CD8+ T cells (Rajala et al., 2015). People without T-LGL also have small CD8+ T cell clones with a similar spectrum of somatic GOF *STAT3* mutations, including patients with Felty syndrome (Savola et al., 2018), aplastic anemia (Jerez et al., 2013), primary red cell aplasia (Kawakami et al., 2018), multiple sclerosis, but also in healthy controls (Valori et al., 2021) and healthy donors with chronic HTLV-2 infection (Kim et al., 2021). Consequently, it remains unclear whether *STAT3* mutations are cause or consequence of CD8+ T cell clonal expansion and autoimmune disease.

A diverse array of germline *STAT3* GOF mutations cause a spectrum of childhood autoimmune diseases, by mechanisms unclear (Flanagan et al., 2014; Haapaniemi et al., 2015; Milner et al., 2015). The most frequent clinical manifestations are lymphoproliferation (diffuse lymphadenopathy, splenomegaly), autoimmune cytopenias, growth delay, enteropathy, inflammatory skin diseases, interstitial lung disease, and early-onset endocrinopathies (Fabre et al., 2019), but no changes in CD8+ T cells have been reported. The most frequent germline mutations causing *STAT3* GOF syndrome are T716M and P715 L in 17% and 12% of patients, respectively (Flanagan et al., 2014; Milner et al., 2015; Fabre et al., 2019), in the transactivation (TA) domain containing the Y705 phosphorylation site for Janus tyrosine kinases (JAKs). Curiously, while P715 is near to K658 in the SH2-domain interface of pSTAT3 dimers (Becker et al., 1998), neither T716M nor P715 L are present as somatic mutations in 790 cases of T-LGL (Fasan et al., 2013; Jerez et al., 2012; Koskela et al., 2012; Ishida et al., 2014; Qiu et al., 2013; Barila et al., 2019; Kerr et al., 2019; Shi et al., 2018), whereas two patients with germline STAT3 GOF syndrome have the T-LGL SH2 domain mutation K658N (Flanagan et al., 2014; Ding et al., 2017). This dichotomy poses the question of whether *STAT3* GOF mutations in the SH2 and TA domains have different consequences for CD8+ T cells and autoimmunity.

Here, we analyze the consequences for CD8+ T cells of *STAT3* GOF SH2 (K658N) or TA (T716M) domain mutations in the mouse germline and in people with germline STAT3 GOF syndrome. The findings demonstrate that diverse *STAT3* GOF mutations cause oligoclonal accumulation of T-LGL-like effector CD8+ T cells and that the accumulation of these rogue T cells contributes to autoimmune pathology.

RESULTS

Germline GOF *Stat3* mutations cause pathology in mice

Two recurring human *STAT3* GOF mutations were investigated in CRISPR/*Cas9*-engineered mice (Figure 1A). K658N, a somatic mutation in a patient with T-LGL (Koskela et al., 2012), exemplifies SH2 domain mutations dominating T-LGL, but also occurred in the germline in two unrelated children with lymphadenopathy, splenomegaly, autoimmune cytopenia, dermatitis, recurrent upper respiratory infections, and autoimmune enteropathy (Flanagan et al., 2014; Ding et al., 2017). T716M in the TA domain is the most frequent germline mutation in STAT3 GOF syndrome. T716M heterozygous (HET) founders were generated in C57BL/6J mice. Of 279 microinjected C57BL/6 zygotes, 13 pups were born and 2 had a homologously recombined T716M allele. By contrast, of 266 microinjected C57BL/6 zygotes, 9 pups were

Figure 1. Germline *STAT3* GOF mutations in mice cause developmental lethality, reduced weight, skin inflammation, splenomegaly, and lymphadenopathy

(A) STAT3 protein domains, somatic mutations in T-LGL, and germline mutations in STAT3 GOF syndrome or in healthy individuals in the Medical Genome Reference Bank (MGRB).

(B) Number and percentage of offspring from intercrossed HET parents. p < 0.0001 for *Stat3^T716M* and *Stat3^K658N* by Chi-Square test with 2 degrees of freedom.

(C) Kaplan-Meier survival curves using the product-limit method accounting for censored mice. Differences in survival analyzed by log-rank (Mantel-Cox) test, Bonferroni-corrected for multiple comparisons.

(D) Weight of individual mice 10–20 or 40–50 weeks old. Bars: mean and standard deviation (SD).

(E) Number and percentage of mice >7 weeks old exhibiting at least one pathology: skin inflammation, hair loss, ringtail, cataracts, diarrhea. Representative images of *K658N* HOMs.

(F) Mean severity score for hair loss and/or skin inflammation, with age.

(G) Representative H&E of facial (left) or ear pinna (right) skin.

(H) Number of leukocytes per spleen or inguinal lymph nodes. Bars: mean and standard deviation. Representative images of organs shown below.

(D and H) Statistical comparisons by t test with Holm-Sidak correction for multiple comparisons. *p < 0.05; **p < 0.01; ***p < 0.001.

born but none carried the homologously recombined K658N allele. However, from 129 (C57BL/6J × FVB/J) F_2 hybrid zygotes microinjected with the same sgRNA and targeting oligonucleotide, 19 pups were born and 2 had K658N alleles. This could reflect Poisson sampling or that the viability of $Stat3^{K658N}$ mutant animals may require a unique aspect of the hybrid genotype.

Following intercross of *T716M* or *K658N* HETs, weaned homozygotes (HOM) were observed at less than half the expected Mendelian frequency (Figure 1B). 20% of *K658N* HOMs died or required ethical culling by age 7 weeks, and 50% by age 25 weeks (Figure 1C). *K658N* HETs had an intermediate survival defect, as did *T716M* HOM relative to HET mice (Figure 1C). At 10–20 and 40–50 weeks of age, $Stat3^{T716M}$ and $Stat3^{K658N}$ mutants weighed less than wild-type (WT) littermates, and 40-to-50-week-old HETs had median weights between WT and HOMs (Figure 1D).

From 3 to 5 weeks of age, *K658N* HOMs were smaller, hunched, less active, and had red, flaky ears and variable hair loss around the eyes, snout, neck, and tail (Figure 1E). Cataracts, ringtail, and inflamed joints occurred at lower penetrance. This visible, gross pathology was fully penetrant in *K658N* HOMs that survived beyond 7 weeks. Milder skin and eye pathology appeared on average at 15 weeks in 73% of *K658N* HETs (Figures 1E and 1F). Skin pathology was suppressed in $Rag1^{KO/KO}$ $Stat3^{K658N/K658N}$ mice but developed normally in $Rag1^{KO/+}$ $Stat3^{K658N/K658N}$ mice (Figure 1F), indicating a requirement for T or B cells and establishing that STAT3 GOF in keratinocytes is insufficient to cause pathology. *T716M* HOMs presented at 7–25 weeks with cataracts and skin inflammation limited to the ears and tail—a phenotype that occurred at low penetrance in *T716M* HETs at 40–50 weeks.

Comprehensive anatomical and histopathology analysis of *T716M* HOM (n = 3) and WT (n = 3), and *K658N* HOM (n = 5), HET (n = 1) and WT (n = 5) mice revealed consistent abnormalities in keratinized epithelia. All tested *K658N* HOMs had acanthotic epidermal hyperplasia and dermal mononuclear infiltrates including mast cells especially on the face and ears (Figure 1G), tail, penis, and milder dermatitis of distal limbs. All 5 had otitis media with submucosal oedema and large foamy luminal macrophages, and 3/5 displayed acanthosis and lymphocytic or neutrophilic infiltration of the esophageal mucosa. The cause of the wasting syndrome and early death was not apparent from gross or histological analysis.

Splenomegaly and lymphadenopathy—the two most prevalent abnormalities in human germline STAT3 GOF syndrome—were highly penetrant along with blood leukocytosis in K658N or T716M HOMs, while HETs had intermediate increases (Figures 1H and S1A). Circulating, splenic, and bone marrow neutrophils were increased in mutant mice (Figure S1B), indicating that neutropenia, a common T-LGL presentation, did not cause early death of STAT3 GOF mice. The differences in gross pathology may reflect a functional difference between the GOF alleles or differences between C57BL/6 and FVB strains in other genes affecting traits such as skin keratinocyte transformation (Wakabayashi et al., 2007).

Germline STAT3 GOF causes accumulation of NKG2D+ effector CD8+ T cells in mice

We focused on whether *Stat3* GOF mutations were sufficient to dysregulate CD8+ T cells. *T716M* and *K658N* HOMs had

increased frequencies of blood CD8+ relative to CD4+ T cells (Figure S1C) and mildly increased number of CD8+ T cells per spleen (Figure 2A). However, *K658N* and *T716M* HOMs had 8- and 7-fold respective increases in percentage and 13- and 12-fold respective increases in number of CD8+ CD62L− CD44+ effector memory T (TEM) cells (Figures 2B and 2C). *K658N* and *T716M* HETs had intermediate 6- and 2-fold respective increases in number of CD8+ TEMs (Figures 2B and 2C). Thus, both GOF mutations dysregulate CD8+ T cells.

To analyze effector CD8+ T cell dysregulation, we focused on NKG2D for three reasons. First, *Klrk1* (encoding NKG2D) is a STAT3 target in natural killer (NK) cells (Zhu et al., 2014), and NKG2D acts as a costimulatory receptor on CD8+ T cells for stress-induced major histocompatibility complex class I (MHC-class-I)-related proteins MICA and ULBP in humans (Bauer et al., 1999; Wu et al., 1999; Sutherland et al., 2001) and Rae1 and H-60 in mice (Cerwenka et al., 2000; Diefenbach et al., 2000). Second, most CD8+ CD57+ T-LGLs express NKG2D (Bigouret et al., 2003). Third, NKG2D+ CD8+ TEMs cause autoimmune alopecia in C3H/H3J mice, a condition treated by JAK inhibition (Xing et al., 2014). *K658N* and *T716M* mutant mice had a *Stat3* mutant allele dose-dependent increase in percentages of NKG2D-expressing CD8+ TEMs in the blood, bone marrow, and spleen (Figure S1D). Increased CD8+ NKG2D+ T cells in these mice are therefore not explained by increased numbers of CD8+ TEMs. *K658N* and *T716M* HOMs had 20- and 12-fold increases, respectively, in number of spleen NKG2D+ CD8+ T cells, while HETs had 8- and 3-fold increases (Figures 2D and 2E).

To further characterize aberrant NKG2D+ effector CD8+ T cells in STAT3 GOF mice we measured migration, maturation, and activation markers. In WT mice, only 20% of NKG2D+ CD8+ T cells expressed the atypical chemokine receptor CX3CR1, whereas 60% of NKG2D+ CD8+ T cells were CX3CR1+ in HET or HOM mice from either *Stat3* GOF strain. The total number of CX3CR1+ NKG2D+ CD8+ T cells was increased in spleen, bone marrow, and blood (Figures 2F and 2G). Compared with their CX3CR1− counterparts, CX3CR1+ NKG2D+ CD8+ T cells had a distinct protein expression profile in both WT and mutant mice: (1) they had a CD44+ CD62L− KLRG1hi CD27lo CD127lo CXCR3lo phenotype of terminally differentiated effector CD8+ T cells (Figures 2F and S1E) and (2) had the lowest cell-surface TCRβ and CD8 levels among CD8+ T cell subsets, which were further diminished in *Stat3*-mutant mice (Figure S1F) and reminiscent of CD8 and TCR "de-tuning" during CD8+ T cell cytotoxic responses (Xiao et al., 2007).

Germline STAT3 GOF causes accumulation of NKG2Dhi and CD57+ effector CD8+ T cells in humans

To generalize the findings in $Stat3^{GOF}$ mice, we analyzed peripheral blood CD8+ T cells in 11 people with childhood-onset multi-organ autoimmunity and lymphoproliferation caused by germline *STAT3* GOF mutations (listed in Table S1). Flow cytometry of peripheral blood mononuclear cells (PBMCs) revealed normal frequencies of circulating T cells (Figure 3A). However, like $Stat3^{GOF}$ mutant mice, patients had increased CD8+ and decreased CD4+ T cell frequencies and consequent 2-fold decrease in CD4:CD8 ratio, relative to controls (Figure 3B). There were no significant differences in percentages of CD8+ T cells with a CD45RA+ CCR7+
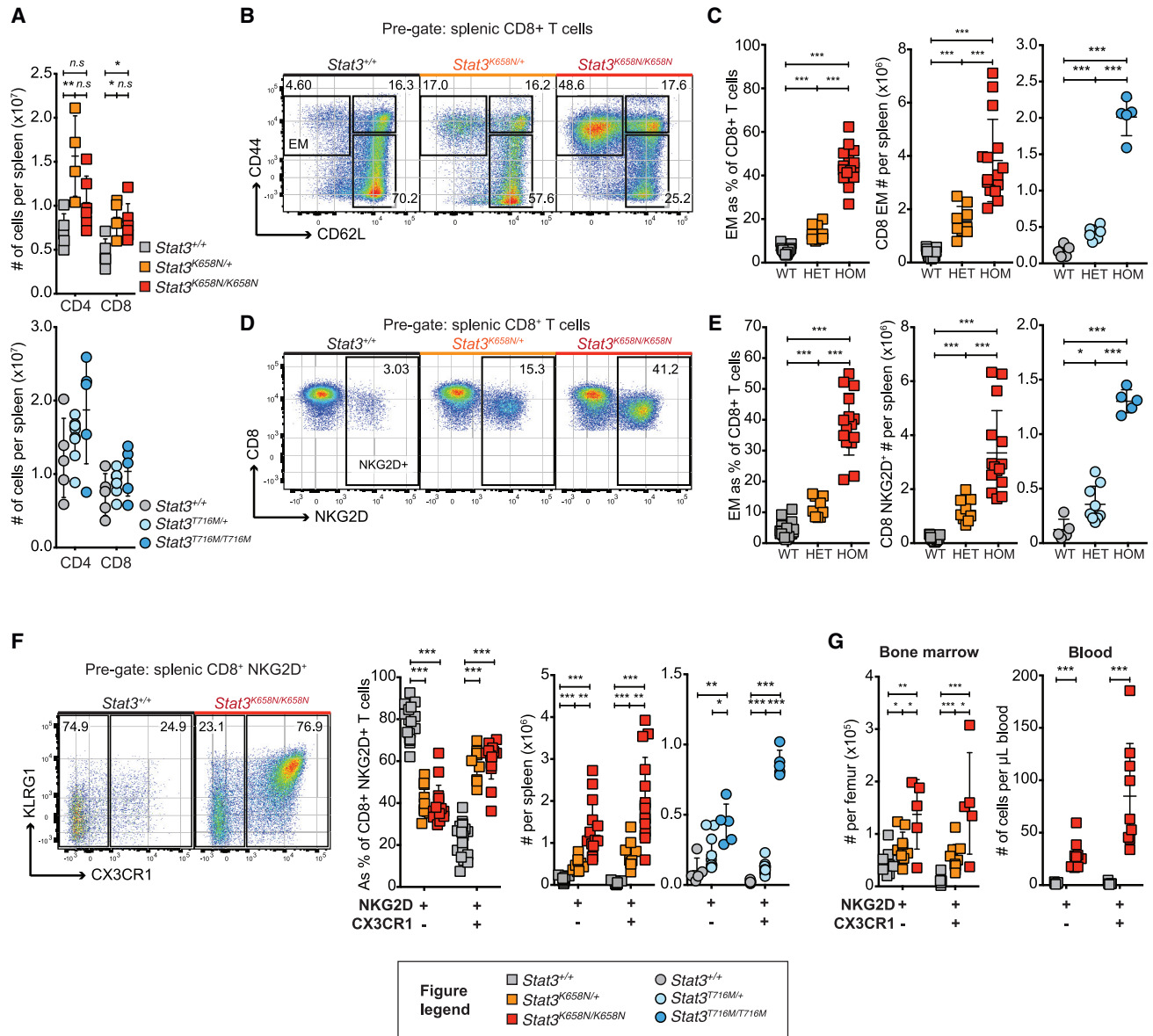
Figure 2. Germline *Stat3* GOF mutations drive accumulation of NKG2D⁺ CX3CR1⁺ KLRG1^high CD8⁺ T cells

(A) Number of CD4⁺ or CD8⁺ T cells per spleen.

(B) Representative plots of splenic CD8⁺ T cells, showing percentage of CD44⁻ CD62L⁺ naive, CD44⁺ CD62L⁺ central memory (CM), and CD44⁺ CD62L⁻ effector memory (EM).

(C) Percent of and number per spleen of CD8⁺ TEM.

(D and E) Representative plots of NKG2D expression by splenic CD8⁺ T cells, percent expressing NKG2D, and number per spleen.

(F) Representative plots of CX3CR1 and KLRG1 on NKG2D⁺ CD8⁺ T cells, percentage of and number per spleen of CX3CR1⁻ or CX3CR1⁺ NKG2D⁺ CD8⁺ T cells.

(G) Number of CX3CR1⁻ or CX3CR1⁺ NKG2D⁺ CD8⁺ T cells per femur or μL blood.

(C–G) Genotypes as per A and key. Symbols: individual animals. Bars: mean ± SD. Statistical comparisons by t test with Holm-Sidak correction for multiple comparisons. *$p < 0.05$; **$p < 0.01$; ***$p < 0.001$. Data representative of > 5 experiments with n > 4 mice per group.

naive, CD45RA⁻ CCR7⁺ central memory, CD45RA⁻ CCR7⁻ effector memory or CD45RA⁺ CCR7⁻ terminal effector memory re-expressing CD45RA (T_EMRA) phenotype (Figure 3C). While all CD8⁺ T cells express NKG2D in humans, we observed a large increase in MFI of NKG2D on patient relative to control CD8⁺ T cells, particularly on T_EMRA CD8⁺ T cells (Figures 3D, S2A, and S2B). Consequently, patients had significantly increased

NKG2D^hi cells as a percentage of CD8⁺ T cells, T cells, or lymphocytes (Figures 3E and S2C). Patients also had a 3-fold increase in frequency of CX3CR1⁺ NKG2D^hi CD8⁺ T cells (Figure 3F). Consistent with T_EMRA and T-LGL cells, CD8⁺ T cells from *STAT3^GOF* patients P9 and P3 had decreased expression of CD28, CD127, CD27, CCR7, and increased CD95, relative to controls (Figure S3A).
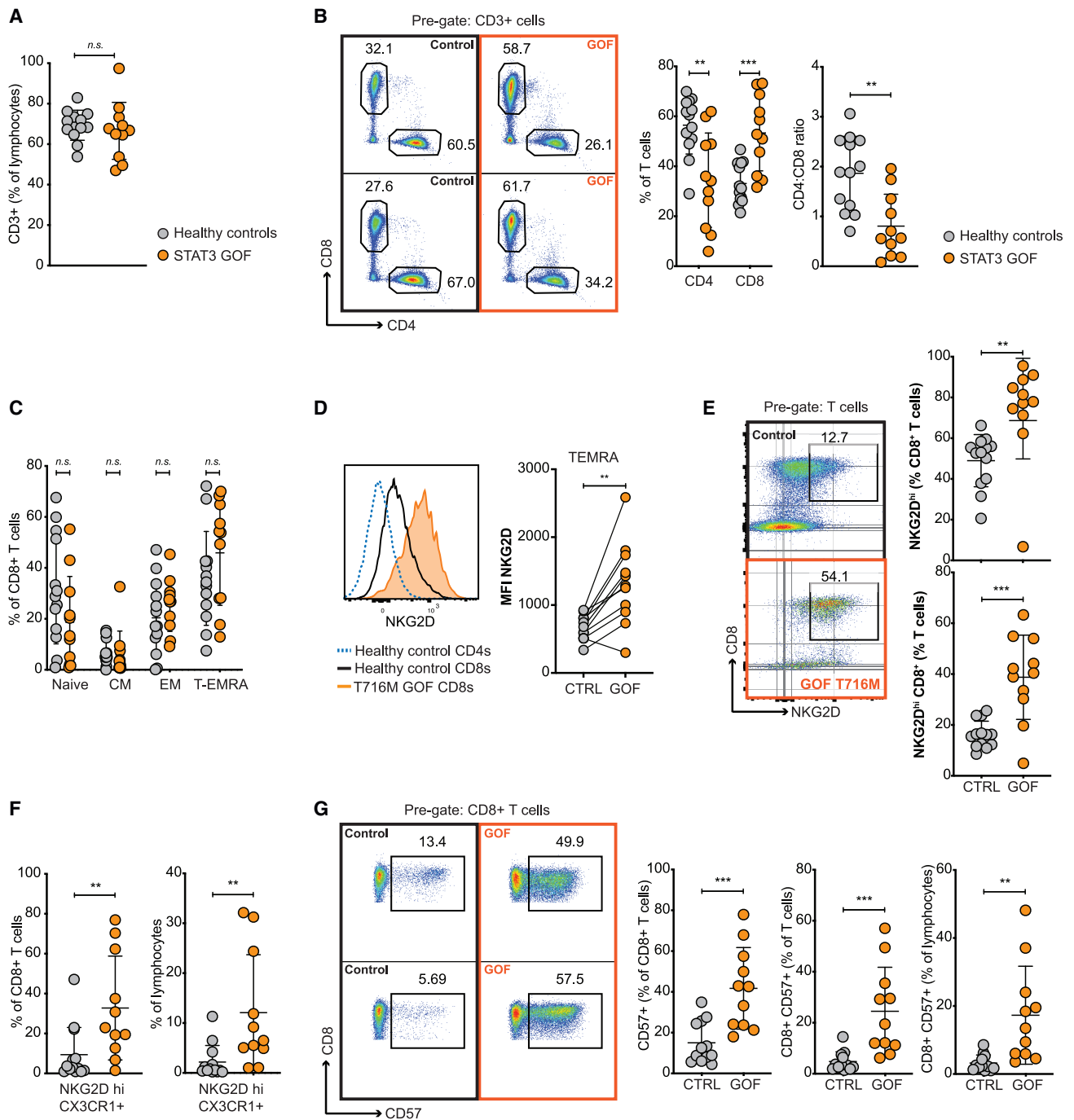
Figure 3. NKG2D^hi CD57^+ effector CD8^+ T cells accumulate in individuals with *STAT3* GOF syndrome

(A–F) Flow cytometry on PBMCs in 13 controls (grey) and 11 patients with germline *STAT3* GOF syndrome (orange).

(A) Percent of CD3^+ lymphocytes.

(B) Percent of CD4^+ or CD8^+ T cells and CD4:CD8 ratio, and representative plots from 2 patients and controls.

(C) Percent of CD8^+ T cells with CD45RA^+ CCR7^+ naive, CD45RA^− CCR7^+ CM, CD45RA^− CCR7^− EM, or CD45RA^+ CCR7^− terminal effector re-expressing CD45RA (T_EMRA) phenotype.

(D) Representative histograms of NKG2D on patient and control CD8^+ and control CD4^+ T cells, and NKG2D mean fluorescence (MFI) on T_EMRA CD8^+ T cells. Lines join samples analyzed in the same experiment. In experiments with multiple controls, grey symbols denote the average of control MFIs.

(E) Representative plots of NKG2D and CD8 on patient and control T cells, and percentage of NKG2D^hi CD8^+ T cells among CD8^+ or total T cells.

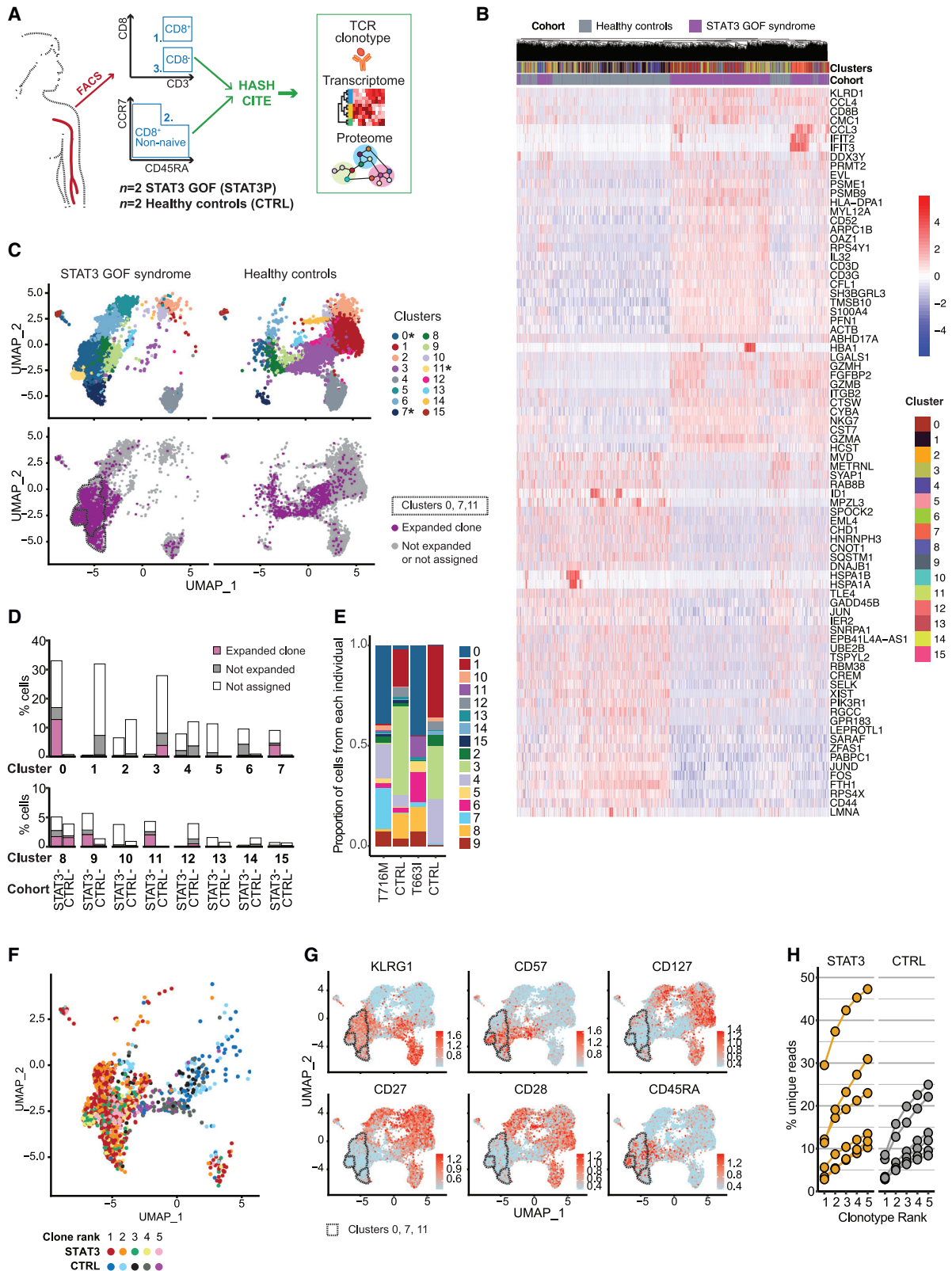(F) Percentage of CX3CR1^+ NKG2D^hi CD8^+ T cells among CD8^+ T cells or lymphocytes.

(G) Representative plots and % CD57^+ CD8^+ T cells among CD8^+ T cells, total T cells or lymphocytes.

(A–G) Data combined from 9 independent experiments. Bars: mean ± SD. Statistical comparisons by t test with Holm-Sidak correction for multiple comparisons.
* p < 0.05; **p < 0.01; ***p < 0.001.

(legend on next page)

Since the majority of T-LGL and a subset of granzyme^hi perforin^hi normal CD8^+ T cells express CD57 (also called HNK-1; Focosi et al., 2010; Chou et al., 1986; Voshol et al., 1996), we measured CD57 in germline *STAT3* GOF patients. Relative to controls, patients had a 3- and 12-fold increase in CD57^+ cells as a percentage of CD8^+ T cells or of circulating lymphocytes, respectively (Figure 3G). In 3 out of 10 patients where these data were obtained, the number of CD57^+ CD8^+ T cells exceeded 0.5×10^9/L (Table S1), the threshold for T-LGL diagnosis when accompanied by autoimmune conditions. In a fourth patient, the number was 0.46×10^9/L (Table S1). The age range was of 12–35 years (mean 22) for patients and 16–84 years (mean 38) for controls (Table S1). Given that CD57^+ CD8^+ T cells accumulate in humans with age (Czesnikiewicz-Guzik et al., 2008), our data may under-estimate the increase in CD57^+ CD8^+ T cells in patients relative to controls. In this limited series of patients, there was no discernible correlation between mutations in different STAT3 domains and the degree of CD57^+ CD8^+ T cell dysregulation (Figure S3B). Thus, germline *STAT3* GOF mutations both within and external to the SH2 domain are sufficient to cause CD57^+ CD8^+ accumulation in humans.

To explore the dysregulated effector/memory CD8^+ T cells in STAT3 GOF syndrome, we performed single-cell receptor and gene expression RNA sequencing (RAGE-seq) (Singh et al., 2019) and cellular indexing of transcriptomes and epitopes by sequencing (CITE-seq) (Stoeckius et al., 2017) on non-naive (excluding CD45RA^+ CCR7^+) CD8^+ T cells sorted by fluorescence-activated cell sorting (FACS) (Figure 4A), along with CD8^− CD4^+ cells, from PBMCs of 2 controls and 2 patients: P10 (T716M mutation) and P9 (T663I SH2 domain mutation). To avoid batch effects, equal mixtures of HASH-tagged patient and control cells were analyzed together in a single reaction, and this repeated for a different patient and control in a separate reaction run simultaneously on the same 10X Chromium chip. We observed no significant change in frequency of NKG2D^hi or CD57^+ CD4^+ T cells in the same patients, so CD4^+ T cells were excluded from further analyses.

Non-naive CD8^+ T cells from patients and controls were transcriptionally distinct (Figure 4B). *STAT3*^GOF cells had significantly increased expression of 768 genes, including 12 *HLA* genes, and decreased expression of 396 genes (Table S2). Among the 40 most increased were genes crucial to CD8^+ effector functions and cytotoxicity (Figure 4B): *GZMA*, *GZMB*, and *GZMH* encode

granzymes; *GNLY* and *PFN1* encode pore-forming proteins granulysin and perforin; *NKG7* encodes a key regulator of cytotoxic granule exocytosis (Ng et al., 2020); *FGFBP2*-encodes the cytotoxic lymphocyte-specific protein co-expressed with perforin (Ogawa et al., 2001); and *HCST* encodes DAP10, the NKG2D adaptor protein that stabilizes its expression (Park et al., 2011) and allows signal transduction upon binding to NKG2D ligands (Wu et al., 1999).

Unsupervised dimensionality reduction analysis of single-cell RNA sequencing (scRNA-seq) data for *STAT3* GOF and control non-naïve CD8^+ T cells identified 16 distinct non-naïve CD8^+ T cell clusters (numbered 0–15) (Figure 4C). Clusters 0, 7, and 11 were >90% constituted of STAT3 patient cells. RAGE-seq revealed most of the cells in these clusters with an assignable TCR V(D)J clonotype were expanded clones, defined as ≥5 cells sharing the same V(D)J clonotypic sequence (Figures 4C and 4D). A larger proportion of patient CD8^+ T cells were in expanded clonotypes relative to controls (60.9% versus 30.3%; 2x2 Fisher exact p = 0.046), and expanded clones were larger on average in patients relative to controls (36.4 versus 14.3 cells).

Cluster 0 was more frequent in both patients relative to controls, whereas cluster 11 appeared unique to P9 with a T663I SH2 domain mutation, and cluster 7 was predominantly from P10 with T716M TA domain mutation (Figure 4E). Clusters 0, 7, and 11 were enriched for the largest T cell clones in STAT3 GOF patients (Figure 4F) and expressed high levels of mRNAs encoding cytotoxic effector functions (*GZMA*, *GZMB*, *GZMH*, *PFN1*, *FGFBP2*, *NKG7*, *CTSW*, *GNLY*, *HCST*, *EFHD2*), inflammatory chemokines and cytokines (*CCL3*, *CCL4*, *CCL5*, *IL32*, *IFNG*), and TCR/co-receptor subunits (*CD8A*, *CD8B*, *CD3G*, *CD3D*, *CD3E*) (Table S3). Clusters 0, 7, and 11 were distinguished by high levels of cell surface CD57 and CD45RA and low levels of CD55, CD28, CD27, and CD62L (Figure 4G and Table S3). Collectively, these results demonstrate that a distinct subset of clonally expanded killer effector CD8^+ T cells is increased in human STAT3 GOF syndrome.

We explored the frequencies of clonally expanded NKG2D^hi CD8^+ T cells from additional STAT3 GOF patients by deep *TCRB* VDJ mRNA sequencing of sorted NKG2D^hi CD8^+ T cells from 6 patients and 6 controls (Figure 4H). The largest clonotypes in the patients accounted for 2.8%–29.5% of unique transcripts (mean 10.80%) and compared with 2.8%–8.5% (mean 4.7%) for controls. The 5 largest clonotypes accounted for

---

Figure 4. Clonally expanded CD57^+ effector CD8^+ T cells expressing numerous killer cell genes in STAT3 GOF syndrome patients

(A) Workflow for analyzing non-naive CD8^+ T cells from 2 controls and 2 STAT3 GOF patients, P10 (T716M) and P9 (T663I), by single cell TCR, transcriptome, and surface protein sequencing. To avoid batch effects, equal mixtures of HASH-tagged patient and control T cells were analyzed together in a single reaction, and this repeated for a different patient and control in a separate reaction run simultaneously on the same 10X Chromium chip.

(B) Unsupervised clustered heatmap of single non-naive CD8^+ T cells (columns) and relative expression (heat key, log2) of the top 40 increased and decreased mRNAs (rows) in patient versus control cells (Cohort key).

(C) UMAPs following mRNA expression dimensionality reduction analysis. Top: each cell is denoted by a dot, color-coded into 16 subsets (0–15) identified by graph-based clustering using K nearest neighbor (Cluster key). Bottom: colored cells are expanded clones based on TCR V(D)J clonotyping.

(D) Percent of non-naive CD8^+ T cells in patients (STAT3) or controls (CTRL) assigned to clusters 0–15 and fraction in each cluster of expanded TCR clones of ≥5 cells.

(E) Relative proportions of clusters 0–15 in patients and controls.

(F) UMAP showing the 1–5 largest TCR clones, within patients (STAT3) or controls (CTRL).

(G) UMAPs displaying relative expression of surface proteins on non-naïve CD8^+ T cells from CITE-seq. Dashed outlines denote clusters 0, 11, and 7 from top to bottom.

(H) Deep *TCRB* VDJ mRNA sequencing of sorted NKG2D^hi CD8^+ T cells from 6 STAT3 GOF patients and 6 controls, showing percentage of *TCRB* transcripts accounted for by the 5 largest clonotypes in each sample. Wilcoxon rank sum test for lower control than STAT3 GOF patient mean p = 0.155.

Figure 5. STAT3 GOF NKG2D⁺ CX3CR1⁺ CD8⁺ T cells in mice overexpress a suite of killer cell genes

(A) Schematic: scRNA-seq on sorted NKG2D⁺ CX3CR1⁺ and NKG2D⁻ CX3CR1⁻ CD8⁺ T cells from $Stat3^{K658N/K658N}$, $Stat3^{T716M/T716M}$ and $Stat3^{+/+}$ mice.

(B) Volcano plot of log2 expression fold-change (log2FC) versus moderated t-statistic for differentially expressed genes (FWER < 0.05 using $limma$) in NKG2D⁺ CX3CR1⁺ CD8⁺ T cells relative to NKG2D⁻ CX3CR1⁻ (total) CD8⁺ T cells in $Stat3^{T716M/T716M}$ mice. Text: mRNAs of interest.

(C) mRNAs significantly increased (FWER < 0.05; log2FC > 0.2) in both $Stat3^{K658N/K658N}$ and $Stat3^{T716M/T716M}$ NKG2D⁺ CX3CR1⁺ CD8⁺ T cells relative to matched $Stat3^{+/+}$ cells.

(D) Violin plots of kernel density estimations of $Gzma$, $Gzmb$, and $Gzmk$ mRNA log2 normalized counts per million (CPM) per cell in NKG2D⁺ CX3CR1⁺ CD8⁺ T cells. Dots: median. Lines: interquartile range.

10.3%–47.3% of unique transcripts (mean 22.8%) in patients and 8.4%–24.9% in controls (mean 15.1%). Thus, large clonal CD8^{+} T cell expansions occur in germline *STAT3* GOF patients and in healthy people.

Accumulating NKG2D^{+} CD8^{+} T cells in *Stat3* GOF mice over-express cell cycle and killer cell genes

To complement the human analysis, scRNA-seq was performed on flow-sorted spleen NKG2D^{+} CX3CR1^{+} CD8^{+} T cells from *T716M* HOM, *K658N* HOM, and WT mice (Figure 5A). For comparison, total CD8^{+} T cells were also sorted from *T716M* HOM and WT littermates. During UMAP analysis, cells within the total CD8^{+} T cell population that clustered with sorted NKG2D^{+} CX3CR1^{+} CD8^{+} T cells were excluded prior to differential gene expression analysis. In *Stat3*[T716M/T716M] mice, NKG2D^{+} CX3CR1^{+} CD8^{+} T cells differentially expressed 4667 genes compared to total CD8^{+} T cells from the same mice (Figure 5B and Table S4). RNAs encoding the two markers used for sorting, *Klrk1* and *Cx3cr1*, were the first and third most increased in the sorted cells, validating the analysis. NKG2D^{+} CX3CR1^{+} CD8^{+} T cells also had increased mRNAs encoding perforins, granzymes, interferon gamma, chemokines, NK cell-associated receptor and signaling molecules, and *Zeb2*, *Prdm1*, *Id2*, *Eomes*, and *Stat4* mRNAs encoding transcription factors that promote memory/effector CD8^{+} T cell differentiation (Figure 5B and Table S4). Thus, dysregulated effector memory CD8^{+} T cells in STAT3 GOF mice display a gene expression profile of killer effectors.

The consequences of STAT3 GOF within this killer subset were explored by differential gene expression between *Stat3*-mutant and WT NKG2D^{+} CX3CR1^{+} CD8^{+} T cells. There were 1,918 genes significantly (FWER < 0.05) increased and 571 decreased in *T716M* HOM (Table S5), and 216 genes increased and 18 decreased in *K658N* HOM relative to WT NKG2D^{+} CX3CR1^{+} CD8^{+} T cells (Table S6). Of these, 94 mRNAs were increased by log2FC > 0.2 in both STAT3 GOF mutants including *Gzmb*, a STAT3 target in activated CD8^{+} T cells (Lu et al., 2019), *Gzma*, and *Gzmk* and inflammatory chemokines *Ccl6* and *Ccl9* (Figures 5C and 5D). Gene set enrichment analysis (GSEA) comparing *Stat3*-GOF versus WT NKG2D^{+} CX3CR1^{+} CD8^{+} T cells revealed a skew in mutant cells to increased expression of HALLMARK gene sets associated with the G2M cell cycle checkpoint, E2F transcription factor targets, mRNAs elevated in effector relative to naive or relative to memory CD8^{+} T cells during viral infection (Kaech et al., 2002) (Figures 5E and 5F and Table S7). The most enriched gene set in *K658N* HOM relative to WT NKG2D^{+} CX3CR1^{+} CD8^{+} T cells was of mRNAs increased in CD44^{+} CD8^{+} T cells that were NKG2D^{+} versus NKG2D^{−}, from lymph nodes of autoimmune alopecic C3H/HeJ mice (Xing et al., 2014) (Figures 5G and Table S7).

We validated selected gene expression changes at the protein level by flow cytometry. Relative to WT counterparts, splenic *Stat3*[T716M/T716M] NKG2D^{+} CX3CR1^{+} CD8^{+} T cells expressed

higher levels of *Cx3cr1* mRNA (Figure S4A) and CX3CR1 protein (Figure S4B). Similarly, *Stat3*-mutant NKG2D^{+} CX3CR1^{+} CD8^{+} T cells expressed higher *Klrc1* (encodes NKG2A), *Klrc2* (encodes NKG2C), and *Klrg1* mRNA levels and correspondingly higher NKG2A/C/E and KLRG1 levels (Figures S4C–S4E). Thus, germline STAT3 GOF causes accumulation in mice and humans of NKG2D^{+} effector CD8^{+} T cells over-expressing mRNAs and proteins required for effector and killer functions.

Accumulating NKG2D^{+} CD8^{+} T cells in STAT3 GOF mice comprise many expanded clones

A key question was whether accumulating NKG2D^{+} CD8^{+} T cells in *Stat3* GOF mice comprised a single leukemic clone. In WT and *Stat3*-GOF mice, the percentage of CD8^{+} T cells expressing NKG2D was higher in bone marrow relative to spleen (Figure 6A), increased with age in spleen and blood (Figure 6B) but did not accumulate in frequencies consistent with leukemia. To analyze clonality, we performed TCR mRNA deep sequencing on splenic NKG2D^{−} and NKG2D^{+} CD8^{+} T cells flow sorted from *T716M* (30–45 weeks old) and *K658N* (10–20 weeks old) mice. NKG2D^{+} CD8^{+} T cells from STAT3 GOF or WT mice were highly polyclonal, although the most frequent clonotype accounted on average for 26.40% (range 5.58%–88.2%) relative to 14.70% (range 2.06%–47.70%) of unique *TCRA* reads in mutant relative to WT mice, respectively (Figure 6C). In mutant and WT mice, 50% of unique TCR reads came from less than 50 different clonotypes (Figure 6C) indicating that many large clones contribute to this subset. *Stat3*-mutant NKG2D^{+} CD8^{+} T cells were therefore not a clonal neoplasm, but the presence of many expanded clones among NKG2D^{+} CD8^{+} T cells was reflected by less diversity (measured by Shannon entropy) compared with NKG2D^{−} CD8^{+} T cells (Figure 6D). A similar pattern of clonotype distribution frequencies was observed following *TCRA* and *TCRB* deep sequencing of NKG2D^{+} CX3CR1^{+} CD8^{+} T cells from *Stat3*[K658N/K658N] mice (Figure 6E). These results parallel the presence of many expanded clones in non-naive CD8^{+} clusters 0, 7, and 11 in *STAT3* GOF patients (Figure 4), and resemble observations for CD57^{+} relative to CD57^{−} CD8^{+} T cells in humans (Morley et al., 1995). Given that the total number of NKGD2^{hi} or CD57^{+} CD8^{+} T cells was dramatically increased in mice or humans with germline *STAT3* GOF, these results indicate that these mutations are insufficient alone to cause monoclonal T-LGL but enhance accumulation of many large effector CD8^{+} T cell clones.

NKG2D and IL-2/IL-15 receptors drive accumulation of NKG2D^{+} CD8^{+} T cells in STAT3 GOF mice

To identify pathways essential for polyclonal expansion of STAT3 GOF NKG2D^{+} CD8^{+} T cells, we tested whether they were diminished in *Stat3* GOF mice by genetically or pharmacologically interfering with CX3CR1, IL10R, NKG2D, IL6R, IL21R, IL7R, or IL2/IL15RB. Homozygous germline *Cx3cr1* deletion resulted in a variable, small decrease in percentage of splenic NKG2D^{+} CD8^{+} T cells in *Stat3*[K658N] mutants (Figure S5A). CX3CR1

(E–G) GSEA of enrichment score (y axis) for rank-ordered genes (x axis) in *Stat3*[K658N/K658N] versus *Stat3*^{+/+} or *Stat3*[T716M/T716M] versus *Stat3*^{+/+} NKG2D^{+} CX3CR1^{+} CD8^{+} T cells.

(E) HALLMARK gene sets G2M_CHECKPOINT (#M5901) or E2F_TARGETS (#M5925).

(F) Immunologic term gene set KAECH_DAY8_EFF_VS_MEMORY_CD8_TCELL_UP (#M3027).

(G) Set of mRNAs increased in NKG2D^{+} compared with NKG2D^{−} CD8^{+} T cells from mouse autoimmune alopecia (Xing et al., 2014).
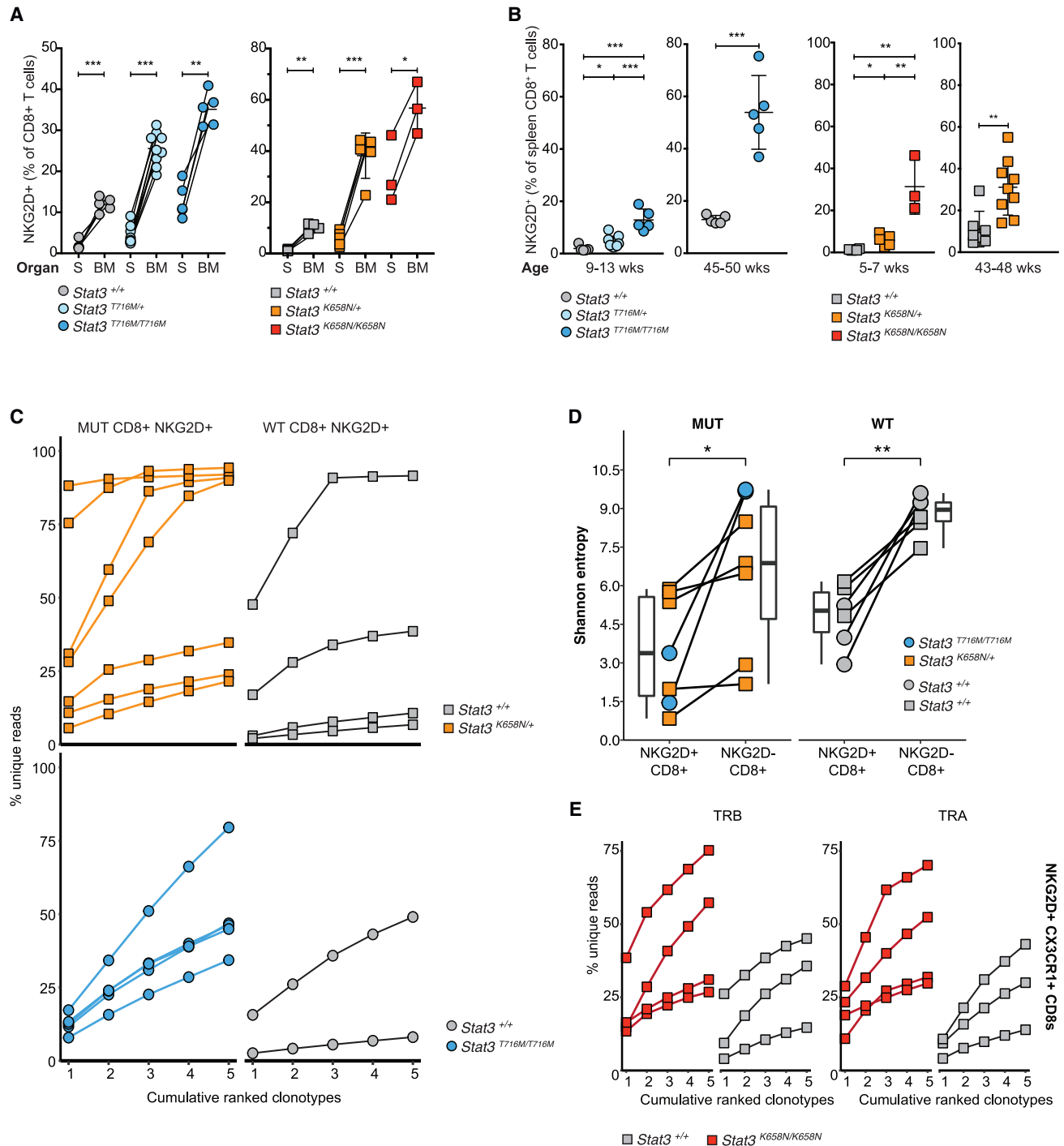
Figure 6. Oligoclonal *Stat3*-mutant CD8⁺ NKG2D⁺ T cells accumulate in the spleen, blood, and bone marrow with age

(A) Percent of NKG2D⁺ spleen or bone marrow CD8⁺ T cells. Lines link measurements from the same mouse. Statistical analysis by paired t test.

(B) Percent of NKG2D⁺ splenic CD8⁺ T cells, with age. Statistical analysis by t test corrected for multiple comparisons by Holm-Sidak. Bars: mean ± SD.

(C–E) Deep TCR V(D)J mRNA sequencing by 5'RACE from sorted NKG2D⁻ and NKG2D⁺ splenic TCRβ⁺ CD8⁺ T cells.

(C) Cumulative percent of unique *TCRA* reads (y axis, determined using unique molecular identifiers UMIs) contributed by top 5 ranked clonotypes (x axis) in individual mice.

(D) Shannon Entropy calculations of *TCRA* repertoire diversity. Lines join data from the same mouse. Boxplots: median and interquartile range.

(E) Cumulative percent of unique *TCRB* or *TCRA* reads contributed by top 5 ranked clonotypes in sorted CX3CR1⁺ NKG2D⁺ CD8⁺ T cells. p values are independent, calculated by Wilcoxon rank-sum test. *p < 0.05; **p < 0.01; ***p < 0.001.
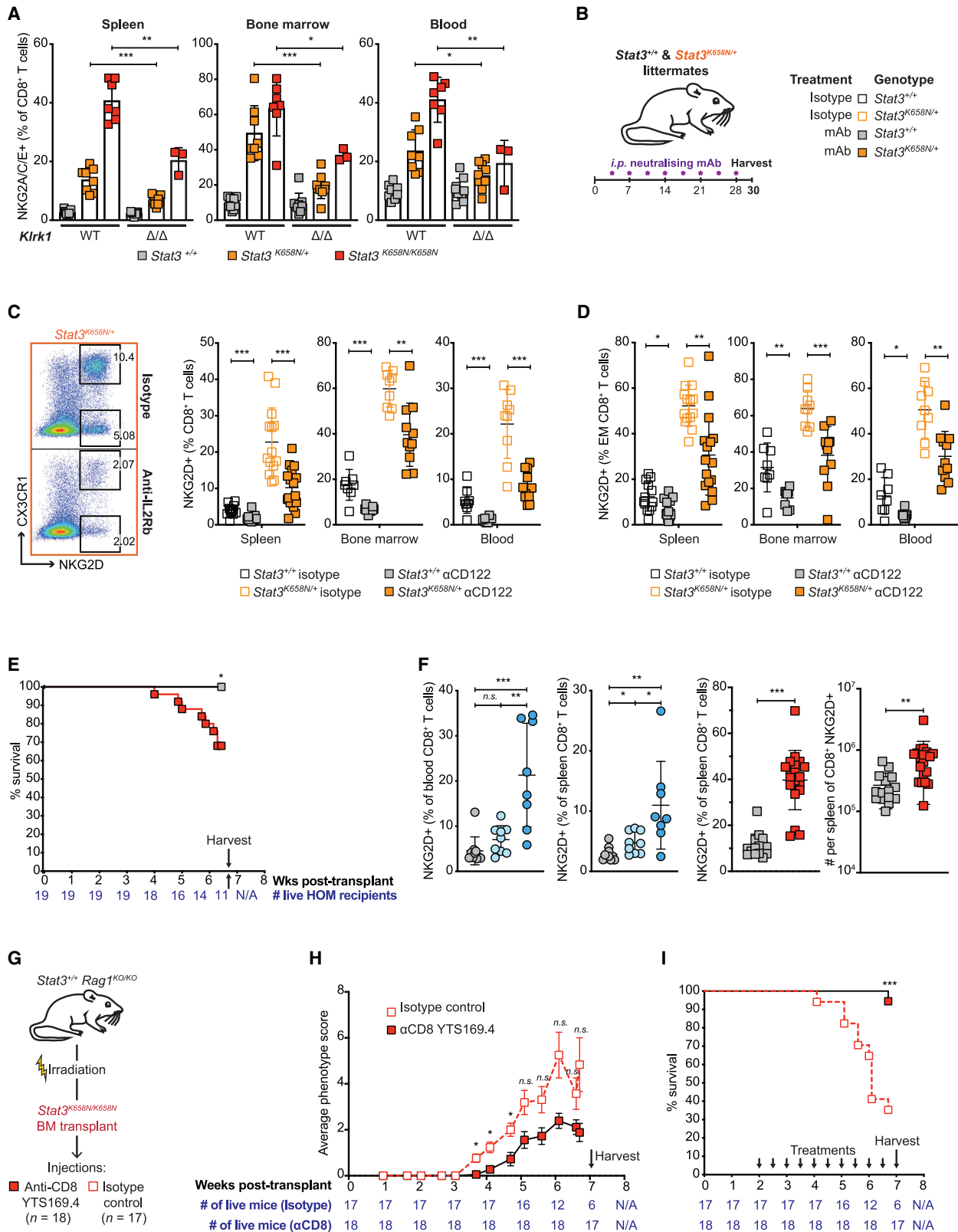
expression on NKG2D+ CD8+ T cells is largely restricted to a CD27lo KLRG1hi CD62Lneg subset (Figures S5B and S5C), but we observed no decrease in this subset between *Cx3cr1*+/+ and *Cx3cr1*KO/KO mice (Figure S5D).

The STAT3-signalling cytokine interleukin 10 (IL-10) decreases inflammation and antigen-induced CD8+ T cell activation (Smith et al., 2018). However, in the absence of the essential IL-10RA, in *Stat3*T716M/T716M *Il10ra*KO/KO relative to *Stat3*T716M/T716M *Il10ra*+/+ mice, there was no significant change in percentage of NKG2D+ cells within CD8+ TEM cells (Figure S5E).

We crossed *Stat3*K658N mice to *Klrk1*Δ mice lacking NKG2D. Most NKG2D+ CD8+ T cells in *Stat3* GOF mice co-express NKG2A/C/E, which we thus used as a proxy for NKG2D (Figure S5F). *Klrk1*KO/KO *Stat3*K658N/K658N mice had reduced frequencies of NKG2A/C/E+ CX3CR1+ CD8+ T cells in spleen, bone marrow, and blood compared with *Klrk1*+/+ *Stat3*K658N/K658N mice (Figure 7A and data not shown). NKG2D therefore contributes to *STAT3*-mutant effector CD8+ accumulation, but NKG2D deficiency is insufficient to fully suppress accumulation of these cells in *Stat3* GOF compared with *Stat3* WT mice.

Pharmacologic interference was performed by treating *Stat3*K658N HETs with monoclonal antibodies (mAbs) blocking different cell-surface receptors (Figure 7B). Consistent with results in *Klrk1*KO mice, *Stat3*K658N mice treated with a blocking anti-NKG2D mAb had decreased NKG2A/C/E+ CX3CR1+ CD8+ T cells relative to control mAb-treated mice (Figure S5G). Flow cytometric analysis of ear cell suspensions revealed higher staining of CD45neg cells from *Stat3* mutant mice with mAb to the NKG2D-ligand murine UL16-binding protein like transcript (MULTI; Figure S5H).

Blocking IL-6R or IL-21R signaling to STAT3 or IL-7R signaling to STAT5 using mAbs, had no significant effect on the frequency of NKG2D+ CD8+ T cells (Figures S5I and S5J). By contrast, *Stat3*K658N mice treated with anti-CD122 blocking mAb, targeting the IL-15R/IL-2Rβ chain required for IL-15 and IL-2 signaling, had half as many NKG2D+ cells among all CD8+ T cells (Figure 7C) or among CD8+ TEM cells (Figure 7D) in the spleen, bone marrow, and blood compared with control mAb-treated mice. To test the specific role of IL-2 in the accumulation of *Stat3*K658N/+ NKG2D+ CD8+ T cells, *Stat3*+/+ and *Stat3*K658N/+ mice were treated with anti-IL-2 mAbs S4B6-1 and JES6-1A12 that selectively block the high- and low-affinity IL-2R binding sites, respectively, of the IL-2 molecule (Boyman et al., 2006). Due to Treg cell dependence on IL-2 (Boyman et al., 2006), the pair of IL-2 blocking antibodies significantly depleted Tregs in WT and *K658N* HETs relative to animals given control mAbs (Figure S6A). However, IL-2 blockade caused no change in frequency or total number of splenic NKG2D+ CD8+ T cells, relative to WT and *Stat3*K658N/+ mice treated with control mAbs (Figure S6B). Collectively, these findings establish that NKG2D and IL-15R/IL-2Rβ are required for maximal accumulation of NKG2D+ CD8+ T cells bearing pathogenic *STAT3* GOF mutations, whereas IL-2, IL-6, IL-7, IL-10, and IL-21 appear individually dispensable.

IL-15 can increase CD8+ T cell NKG2D expression and innate-like cytotoxicity (Kim et al., 2018) and induce NKG2D expression within TCR-activated CD8+ T cells (Roberts et al., 2001; Meresse et al., 2004). We therefore tested whether *STAT3* GOF alters CD8+ T cell sensitivity to recombinant IL-15 or anti-CD3, measured by increased NKG2D on splenic naive and effector CD8+ T cells FACS-purified from *Stat3*+/+ and *Stat3*T716M/T716M mice. *T716M* HOM naive and effector CD8+ T cells showed comparable NKG2D induction to WT cells in response to low or high dose IL-15 or IL-15 plus anti-CD3 (Figures S6C and S6D).

Depleting *STAT3* GOF CD8+ T cells ameliorates inflammation and lethality

Pathology in humans and mice with germline *STAT3* GOF syndrome may be due to STAT3 GOF in non-hematopoietic cells. We therefore generated chimeric mice with hematopoietic-restricted *Stat3* GOF mutations by transplanting *Stat3*+/+ *Rag1*KO/KO mice with *Stat3*-GOF or WT bone marrow (Figure S7A). Mice transplanted with *Stat3*-GOF but not WT marrow developed a range of gross pathologies (Figure S7B). Recipients of either *T716M* HOM or *K658N* HOM marrow developed lymphadenopathy, splenomegaly, and/or cataracts. *K658N* HOM marrow recipients also developed hair loss around the eyes, ventral hair loss, diarrhea, weight loss requiring ethical culling, or were unexpectedly found dead. Eight of 25 *K658N* HOM marrow recipients required sacrifice at ethical end-point within 7 weeks post-transplant compared with 0 of 15 WT marrow recipients (Figure 7E). NKG2D+ CD8+ T cells were increased in *T716M* or *K658N* HOM marrow recipients (Figure 7F).

To test the role of STAT3GOF CD8+ T cells in the pathology of *K658N* HOM marrow transplant recipients, CD8+ T cells were selectively depleted by injections of anti-CD8 mAb or isotype control mAb starting 2 weeks after transplant (Figure 7G). *K658N* HOM marrow recipients in the control arm started

---

Figure 7. Essential roles of NKG2D and CD122/IL-15Rβ in STAT3 GOF effector CD8+ T cell accumulation and of CD8+ T cells in lethal pathology

(A) Percent of NKG2A/C/E+ cells among spleen CD8+ T cells of *Klrk1*+/+ (WT) or *Klrk1*KO/KO (Δ/Δ) mice. Data pooled from 2 independent experiments.

(B) Schematic of pharmacological blocking experiments.

(C and D) Representative plots of NKG2D+ splenic CD8+ T cells and percent of NKG2D+ among CD8+ cells (C) or CD44hi CD62L− effector memory CD8+ T cells (D) in *Stat3*+/+ or *Stat3*K658N/+ mice treated with isotype or anti-CD122 mAb. Data pooled from n = 3 experiments.

(E) Kaplan-Meier survival curves for *Stat3*+/+ *Rag1*KO/KO recipients transplanted with *Stat3*+/+ (black, n = 15) or *Stat3*K658N/K658N (red, n = 19) bone marrow.

(F) Percent and number of NKG2D+ CD8+ T cells in blood or spleen of *Stat3*+/+ *Rag1*KO/KO marrow transplant recipients. Data representative of 2 experiments with n > 5 mice per group.

(G) Experimental design for selectively depleting STAT3 GOF CD8+ T cells from *Stat3*K658N/K658N transplant recipients.

(H and I) Mean and SD pathology phenotype score and Kaplan-Meier survival curves for the treated mice in (G). Numbers of mice in both treatment arms at different timepoints shown below.

(A, C, D, and F). Statistical comparisons by t test, with Holm-Sidak correction for multiple comparisons. Bars: mean ± SD.

(E and I) Statistical analysis by product-limit method accounting for censored mice, significance calculated by log-rank test. (G) Statistical analysis by two-way ANOVA and Šidák's multiple comparisons test. *p < 0.05; **p < 0.01; ***p < 0.001.

developing gross pathology 3–5 weeks post-transplant at the time that mature T cells reconstitute from hematopoietic stem cells, but the pathology was diminished in recipients treated with anti-CD8 (Figure 7H). By 7 weeks, 11 out of 17 recipients in the isotype control arm died or were ethically culled for weight loss and wasting disease compared to only 1 out of 18 recipients in the CD8$^+$ T cell depleted arm (Figure 7I). Thus, hematopoietic-restricted STAT3 GOF is sufficient to cause accumulation of NKG2D$^+$ CD8$^+$ T cells and to cause lethal pathology requiring CD8$^+$ T cells.

DISCUSSION

The findings here illuminate a pathogenic mechanism in autoimmune disease by resolving a key question about the intersection between cancer and autoimmunity: whether *STAT3* GOF somatic mutations that recur in LGL CD8$^+$ cells are a cause or an effect of clonal expansion and accompanying autoimmune disease. Clone size reflected by mutated *STAT3* variant allele frequency (VAF) in CD8$^+$ T cells varies widely in different human diseases: 0.6%–51% in T-LGL (Rajala et al., 2015), 1%–8% in Felty syndrome (Savola et al., 2018), and 1.1%–16% in primary red cell aplasia (Kawakami et al., 2018). Clones representing 20% of cells (10% VAF for HET mutations) are within the physiological range for effector memory CD8$^+$ T cells (Posnett et al., 1994) and not in the magnitude of leukemias. Moreover, *STAT3* GOF mutations are found in CD8$^+$ T cells of healthy people with VAFs of 0.4%–1.9% and asymptomatic HTLV-infected people with VAFs of 0.5%–11.9% (Valori et al., 2021; Kim et al., 2021). Here, we showed that germline STAT3 GOF mutations did not perturb the preponderant population of naive CD8$^+$ T cells, consistent with mouse bone marrow retroviral transduction experiments (Couronne et al., 2013; Dutta et al., 2018). Instead, they selectively drove expansion of a normally minor subset of effector CD8$^+$ T cells resembling T-LGL cells, strongly expressing CD57 and genes for cytotoxic granule proteins, and highly variable in size of expanded clones. CD8$^+$ T cells bearing a STAT3 GOF SH2-domain mutation were required for lethal inflammatory disease but could also accumulate without causing disease. By revealing that these cells expressed high levels of NKG2D and DAP10/*HSCT* and depended on NKG2D and IL-15R/IL2Rβ for maximal accumulation, the findings here frame a hypothesis explaining their indolent clonal expansion, NK-like effector gene expression profile, and the variable co-occurrence of autoimmune disease.

The partial requirement for NKG2D by STAT3 GOF effector CD8$^+$ T cells is consistent with its role as a costimulatory receptor that activates PI3K signaling (Wu et al., 1999). NKG2D ligands are surface proteins evolutionarily related to MHC class I (Bauer et al., 1999; Wu et al., 1999; Raulet et al., 2013), whose expression is induced by infection, DNA damage, oncogenic mutations, endoplasmic reticulum stress, and inflammatory cytokines (Raulet et al., 2013). Combined triggering by TCR and NKG2D enhances CD8$^+$ T cell proliferation *in vitro* (Groh et al., 2001; Jamieson et al., 2002) and increases clonal expansion of CD8$^+$ T cells bearing TCRs against an MHC-class-I-presented pancreatic islet autoantigen in diabetes-prone NOD mice where NKG2D ligand *Raet1* is constitutively expressed (Ogasawara et al., 2004). STAT3 may induce NKG2D; *KLRK1* is a direct STAT3

target in NK cells (Zhu et al., 2014) and NKG2D levels were higher on STAT3 GOF patient CD8$^+$ T cells.

The TCR specificity of expanded STAT3 GOF CD8$^+$ T cells may shape clonal expansion and patterns of pathology. An MHC haplotype promoting autoimmune diabetes is essential for diabetes acceleration in NOD mice with a different *Stat3* GOF mutation, K392R in the DNA-binding domain (Warshauer et al., 2021). Multiple STAT3 GOF CD8$^+$ clones with different TCRs may contribute to pathology in a cooperative manner, given that T-LGL patients with two or more independent *STAT3*-mutant CD8$^+$ clones have higher incidence of RA relative to patients with a single mutant clone (Rajala et al., 2015).

The finding that CD122 but not IL-2 blockade diminished STAT3 GOF CD8$^+$ effector accumulation is consistent with the role of IL-15 in CD8$^+$ T cell effector accumulation. IL-15/IL-15Rα heterodimers, initially displayed on cell surfaces, engage CD122 and IL-2Rγ to activate STAT5 and STAT3 (Waldmann et al., 2020) and are potent drivers of homeostatic CD8$^+$ T cell proliferation *in vivo* (Chertova et al., 2013). IL-15 and IL-15RA expression by dendritic and myeloid cells is essential for accumulation of effector memory CD8$^+$ T cells (Ku et al., 2000; Zhang et al., 1998; Stonier et al., 2008). Large CD8$^+$ clonal expansions develop spontaneously in old mice and their cell division is inhibited by CD122 blockade (Ku et al., 2001). Concentrations of IL-15 systemically, and at sites of inflammation, play important roles in protective immunity but also in autoimmune diseases, many of which are characterized by increased IL-15 levels (Jabri and Abadie, 2015). IL-15 and NKG2D contribute to innate-like cytotoxicity of bystander CD8$^+$ T cells in hepatitis A infection (Kim et al., 2018). Within TCR-activated CD8$^+$ T cells, IL-15 induces NKG2D and *HSCT*/DAP10 expression (Roberts et al., 2001; Meresse et al., 2004), as does high-dose IL-2 (Verneris et al., 2004; Jabri and Abadie, 2015).

The results here imply wider, multifactorial inputs for STAT3 to drive CD8$^+$ effector accumulation. Neither CD122 blockade nor NKG2D-deficiency fully suppressed STAT3 GOF NKG2D$^+$ CD8$^+$ T cells, and NKG2D induction by TCR or IL-15 was not exaggerated in STAT3 GOF CD8$^+$ T cells *in vitro*. While individual blockade of IL-2, IL-6R, IL-7R, IL-10R, and IL-21R had no measurable effect on STAT3 GOF CD8$^+$ T cell effector accumulation, these cytokines may act in concert with IL-15, NKG2D, and TCR stimulation. Interferon-γ (IFNγ) was highly expressed by NKG2D^{hi} STAT3 GOF CD8$^+$ T cells analyzed here and induces IL-15 in macrophages (Doherty et al., 1996) and hair follicles (Xing et al., 2014). Thus, *STAT3* GOF mutations may exaggerate a positive feedback loop where TCR, IL-15, and other costimuli promote accumulation of NKG2D^{hi} IFNγ$^+$ effector CD8$^+$ T cells, which in turn induce NKG2D ligands, more IL-15, and costimuli. Another potential input is *CCL5*, a STAT3 target gene (Yang et al., 2007) highly expressed in STAT3 GOF CD8$^+$ T cells. *CCL5* is induced by NKG2D stimulation of TCR-activated CD8$^+$ T cells and encodes the T cell recruiting chemokine RANTES (Markiewicz et al., 2012).

The experiments here demonstrated that T and/or B cells were necessary for pathology in *K658N* HOM mice, that the mutation restricted to hematopoietic cells was sufficient for lethal pathology, and that CD8$^+$ T cells were necessary. Whether expanded *STAT3*-mutant effector CD8$^+$ T cell clones are *sufficient* for pathology is a separate question. Expanded STAT3 GOF CD8$^+$ T cell clones are found in healthy people and in STAT3 GOF

mice with no skin inflammation or wasting syndrome. In preliminary studies, we adoptively transferred 5×10^6 CD8^{+} T cells from *K658N* HOM mice with skin inflammation into irradiated C57BL/6 or *Rag1*[KO/KO] mice and observed no pathology in recipients after 10 weeks. Expanded *STAT3*-mutant CD8^{+} T cell clones thus appear insufficient for overt pathology within this timeframe. Variable pathology in mice and people with *STAT3* GOF NKG2D^{hi} granzyme^{+} perforin^{+} effector CD8^{+} T cells may reflect three potential co-factors. First, the frequency of these cells, consistent with greater frequency and pathology in HOM relative to HET and K658N relative to T716M mice. Second, variability in induction of NKG2D ligands and IL-15 by cellular stress in target cells (Jabri and Abadie, 2015). Third, the extent to which NKG2D stimulation lowers the threshold for TCR-induced IFN-γ production and cytolysis (Roberts et al., 2001; Billadeau et al., 2003) or for MHC-independent NK-like cytotoxicity (Verneris et al., 2004; Karimi et al., 2005; Meresse et al., 2004).

Elevated NKG2D ligands on inflamed synovium (Groh et al., 2003) may contribute to frequent RA in T-LGL (Koskela et al., 2012; Rajala et al., 2015). IL-15 concentrations are increased in RA synovium (McInnes et al., 1996) and T-LGL serum (Chen et al., 2012), and IL-15 reverses ligand-induced NKG2D down-modulation on CD8^{+} T cells (Groh et al., 2002; Roberts et al., 2001) and induces NKG2D ligands on synoviocytes (Groh et al., 2003). In celiac disease, gluten via IL-15 induces MICA on intestinal epithelial cells. Epithelial MICA returns almost to baseline on a gluten-free diet, except in patients with refractory celiac disease type 2 and clonal expansions of innate lymphocytes often carrying *STAT3* GOF mutations (Meresse et al., 2004; Ettersperger et al., 2016; Cording et al., 2021; Soderquist et al., 2021; Hue et al., 2004). Noxious environmental stimuli may thus influence whether STAT3 GOF CD8^{+} T cells cause pathology.

Collectively, the findings here demonstrate that STAT3 GOF mutations in T-LGL are a cause and not simply a consequence of CD8^{+} effector clonal accumulation and autoimmunity. Further, the results lead to the hypothesis that variable autoimmunity associated with CD8^{+} T cell somatic *STAT3* GOF mutations reflects their exaggeration of a feedforward loop with multiple potential inputs: (1) target cells upregulating NKG2D ligands due to inherited, somatic, and/or environmentally induced abnormalities; (2) target tissues and adjacent myeloid cells upregulating IL-15 and other costimuli in response to these abnormalities and to activated B/T cell infiltration; and (3) accumulation of infiltrating STAT3 GOF CD8^{+} T cells with TCRs targeting autoantigens, and their upregulation of NKG2D and its signaling partner DAP10. This loop has many points where inherited or environmental factors can tip clonal expansion of NKG2D^{hi} effector CD8^{+} T cells into pathological destruction of neutrophils, erythrocytes, joint synovium, islet cells, or skin/intestinal epithelial barriers. Our results highlight the need for deeper testing for CD8^{+} T cell clones with *STAT3* GOF somatic mutations in autoimmune disease, and for stratified clinical trials of STAT3/NKG2D/IL15 inhibitors in T-LGL and autoimmune diseases where these rogue CD8^{+} clones are present.

Limitations of the study

The cause of lethality in the mutant mice was not determined, although leukocyte-restricted STAT3 GOF was shown sufficient and CD8^{+} T cells were necessary. Neutrophil counts were normal or elevated, and histological analysis of many organs did not explain lethality. Systemic markers of inflammation such as interferon response genes may provide future insights. Furthermore, while NKG2D and CD122 were necessary for maximal effector CD8^{+} T cell accumulation in the mutant mice, considerable expansion still occurred when they were individually blocked. The expression and role of NKG2D-ligands, IL-15/IL15RA and their receptors in observed pathology, alone and in combination, should be determined. Lastly, adoptive transfer of *Stat3*-mutant CD8^{+} T cells was insufficient to cause pathology within 10 weeks, raising the question of what co-factors contribute to CD8-dependent pathology. Testing possible co-factors will require multifactorial experimental studies.

STAR★METHODS

Detailed methods are provided in the online version of this paper and include the following:

- KEY RESOURCES TABLE
- RESOURCE AVAILABILITY
  - Lead contact
  - Materials availability
  - Data and code availability
- EXPERIMENTAL MODEL AND SUBJECT DETAILS
  - Human subjects
  - *Mouse* handling, housing and husbandry
  - *Mouse* anatomy and histopathology
  - Mouse *strains*
  - Chimeras
  - *Pathology* phenotype scoring
  - *In vivo* monoclonal neutralising antibody treatments
  - Flow cytometry and cell-sorting
  - Enzymatic digestion of mouse ears for flow cytometric analysis
  - *In vitro* stimulation of splenic effector CD8^{+} T cells
  - Single-cell RNA sequencing using the 10X platform
  - Repertoire and gene expression by sequencing
  - TCR deep sequencing by modified 5'RACE
- QUANTIFICATION AND STATISTICAL ANALYSIS

AUTHOR CONTRIBUTIONS

E.M.−F. designed and performed the majority of experiments; R.B. generated *Stat3*-mutant mice; K.P. and G.R. performed flow cytometry on PBMCs; C.S.M., D.S., G.U., I.C., J.W.L., K.H., K.P., L.K., M.O., M.A.C., M.R.J.S., S.M., S.B., and S.G.T obtained patient peripheral blood samples; M.S. and G.A. contributed to deep sequencing or single-cell multi-omics; G.A., K.J.L.J., and T.J.P performed bioinformatics analyses; E.M.−F., S.G.T., J.H.R., and C.C.G interpreted experiments and wrote the manuscript.

DECLARATION OF INTERESTS

The authors declare no competing interests.

REFERENCES

Andersson, E., Kuusanmaki, H., Bortoluzzi, S., Lagstrom, S., Parsons, A., Rajala, H., Van Adrichem, A., Eldfors, S., Olson, T., Clemente, M.J., et al. (2016). Activating somatic mutations outside the SH2-domain of STAT3 in LGL leukemia. Leukemia 30, 1204–1208. https://doi.org/10.1038/leu.2015.263.

Barila, G., Teramo, A., Calabretto, G., Vicenzetto, C., Gasparini, V.R., Pavan, L., Leoncin, M., Vedovato, S., Frigo, A.C., Facco, M., et al. (2019). Stat3 mutations impact on overall survival in large granular lymphocyte leukemia: a single-center experience of 205 patients. Leukemia. https://doi.org/10.1038/s41375-019-0644-0.

Bauer, S., Groh, V., Wu, J., Steinle, A., Phillips, J.H., Lanier, L.L., and Spies, T. (1999). Activation of NK cells and T cells by NKG2D, a receptor for stress-inducible MICA. Science 285, 727–729.

Becker, S., Groner, B., and Müller, C.W. (1998). Three-dimensional structure of the Stat3beta homodimer bound to DNA. Nature 394, 145–151. https://doi.org/10.1038/28101.

Bigouret, V., Hoffmann, T., Arlettaz, L., Villard, J., Colonna, M., Ticheli, A., Gratwohl, A., Samii, K., Chapuis, B., Rufer, N., and Roosnek, E. (2003). Monoclonal T-cell expansions in asymptomatic individuals and in patients with large granular leukemia consist of cytotoxic effector T cells expressing the activating CD94:NKG2C/E and NKD2D killer cell receptors. Blood 101, 3198–3204. https://doi.org/10.1182/blood-2002-08-2408.

Billadeau, D.D., Upshaw, J.L., Schoon, R.A., Dick, C.J., and Leibson, P.J. (2003). NKG2D-DAP10 triggers human NK cell-mediated killing via a Syk-independent regulatory pathway. Nat. Immunol. 4, 557–564. https://doi.org/10.1038/ni929.

Boyman, O., Kovar, M., Rubinstein, M.P., Surh, C.D., and Sprent, J. (2006). Selective stimulation of T cell subsets with antibody-cytokine immune complexes. Science 311, 1924–1927. https://doi.org/10.1126/science.1122927.

Burnet, M. (1965). Somatic mutation and chronic disease. Br. Med. J. 1, 338–342. https://doi.org/10.1136/bmj.1.5431.338.

Cerwenka, A., Bakker, A.B., Mcclanahan, T., Wagner, J., Wu, J., Phillips, J.H., and Lanier, L.L. (2000). Retinoic acid early inducible genes define a ligand family for the activating NKG2D receptor in mice. Immunity 12, 721–727. https://doi.org/10.1016/s1074-7613(00)80222-8.

Chen, J., Petrus, M., Bamford, R., Shih, J.H., Morris, J.C., Janik, J.E., and Waldmann, T.A. (2012). Increased serum soluble IL-15Ralpha levels in T-cell large granular lymphocyte leukemia. Blood 119, 137–143. https://doi.org/10.1182/blood-2011-04-346759.

Chertova, E., Bergamaschi, C., Chertov, O., Sowder, R., Bear, J., Roser, J.D., Beach, R.K., Lifson, J.D., Felber, B.K., and Pavlakis, G.N. (2013). Characterization and favorable in vivo properties of heterodimeric soluble IL-15.IL-15Ralpha cytokine compared to IL-15 monomer. J. Biol. Chem. 288, 18093–18103. https://doi.org/10.1074/jbc.M113.461756.

Chou, D.K., Ilyas, A.A., Evans, J.E., Costello, C., Quarles, R.H., and Jungalwala, F.B. (1986). Structure of sulfated glucuronyl glycolipids in the nervous system reacting with HNK-1 antibody and some IgM paraproteins in neuropathy. J. Biol. Chem. 261, 11717–11725.

Cording, S., Lhermitte, L., Malamut, G., Berrabah, S., Trinquand, A., Guegan, N., Villarese, P., Kaltenbach, S., Meresse, B., Khater, S., et al.; CELAC network (2021). Oncogenetic landscape of lymphomagenesis in coeliac disease. Gut 71, 497–508. https://doi.org/10.1136/gutjnl-2020-322935.

Couronné, L., Scourzic, L., Pilati, C., Della Valle, V., Duffourd, Y., Solary, E., Vainchenker, W., Merlio, J.P., Beylot-Barry, M., Damm, F., et al. (2013).

STAT3 mutations identified in human hematologic neoplasms induce myeloid malignancies in a mouse bone marrow transplantation model. Haematologica 98, 1748–1752. https://doi.org/10.3324/haematol.2013.085068.

Cui, W., Liu, Y., Weinstein, J.S., Craft, J., and Kaech, S.M. (2011). An interleukin-21-interleukin-10-STAT3 pathway is critical for functional maturation of memory CD8+ T cells. Immunity 35, 792–805. https://doi.org/10.1016/j.immuni.2011.09.017.

Czesnikiewicz-Guzik, M., Lee, W.W., Cui, D., Hiruma, Y., Lamar, D.L., Yang, Z.Z., Ouslander, J.G., Weyand, C.M., and Goronzy, J.J. (2008). T cell subset-specific susceptibility to aging. Clin. Immunol. 127, 107–118. https://doi.org/10.1016/j.clim.2007.12.002.

De Araujo, E.D., Orlova, A., Neubauer, H.A., Bajusz, D., Seo, H.S., Dhe-Paganon, S., Keserű, G.M., Moriggl, R., and Gunning, P.T. (2019). Structural implications of STAT3 and STAT5 SH2 domain mutations. Cancers 11, E1757. https://doi.org/10.3390/cancers11111757.

Deenick, E.K., Pelham, S.J., Kane, A., and Ma, C.S. (2018). Signal transducer and activator of transcription 3 control of human T and B cell responses. Front. Immunol. 9, 168. https://doi.org/10.3389/fimmu.2018.00168.

Diefenbach, A., Jamieson, A.M., Liu, S.D., Shastri, N., and Raulet, D.H. (2000). Ligands for the murine NKG2D receptor: expression by tumor cells and activation of NK cells and macrophages. Nat. Immunol. 1, 119–126. https://doi.org/10.1038/77793.

Ding, Y., Zhang, Y., Wang, Y.P., Zhao, H.Y., Chen, X.M., Xue, X.H., Bai, X.M., An, Y.F., Zhang, Z.Y., Tang, X.M., and Zhao, X.D. (2017). [Clinical and immunological analysis of the patient with autoimmunity due to germline STAT3 gain-of-function mutation]. Zhonghua Er Ke Za Zhi 55, 30–36. https://doi.org/10.3760/cma.j.issn.0578-1310.2017.01.006.

Doherty, T.M., Seder, R.A., and Sher, A. (1996). Induction and regulation of IL-15 expression in murine macrophages. J. Immunol. 156, 735–741.

Dutta, A., Yan, D., Hutchison, R.E., and Mohi, G. (2018). STAT3 mutations are not sufficient to induce large granular lymphocytic leukaemia in mice. Br. J. Haematol. 180, 911–915. https://doi.org/10.1111/bjh.14487.

Ettersperger, J., Montcuquet, N., Malamut, G., Guegan, N., Lopez-Lastra, S., Gayraud, S., Reimann, C., Vidal, E., Cagnard, N., Villarese, P., et al. (2016). Interleukin-15-dependent t-cell-like innate intraepithelial lymphocytes develop in the intestine and transform into lymphomas in celiac disease. Immunity 45, 610–625. https://doi.org/10.1016/j.immuni.2016.07.018.

Fabre, A., Marchal, S., Barlogis, V., Mari, B., Barbry, P., Rohrlich, P.S., Forbes, L.R., Vogel, T.P., and Giovannini-Chami, L. (2019). Clinical aspects of STAT3 gain-of-function germline mutations: a systematic review. J. Allergy Clin. Immunol. Pract. 7, 1958–1969.e9. https://doi.org/10.1016/j.jaip.2019.02.018.

Fasan, A., Kern, W., Grossmann, V., Haferlach, C., Haferlach, T., and Schnittger, S. (2013). STAT3 mutations are highly specific for large granular lymphocytic leukemia. Leukemia 27, 1598–1600. https://doi.org/10.1038/leu.2012.350.

Flanagan, S.E., Haapaniemi, E., Russell, M.A., Caswell, R., Allen, H.L., De Franco, E., Mcdonald, T.J., Rajala, H., Ramelius, A., Barton, J., et al. (2014). Activating germline mutations in STAT3 cause early-onset multi-organ autoimmune disease. Nat. Genet. 46, 812–814. https://doi.org/10.1038/ng.3040.

Focosi, D., Bestagno, M., Burrone, O., and Petrini, M. (2010). CD57+ T lymphocytes and functional immune deficiency. J. Leukoc. Biol. 87, 107–116. https://doi.org/10.1189/jlb.0809566.

Goodnow, C.C. (2007). Multistep pathogenesis of autoimmune disease. Cell 130, 25–35. https://doi.org/10.1016/j.cell.2007.06.033.

Groh, V., Bruhl, A., El-Gabalawy, H., Nelson, J.L., and Spies, T. (2003). Stimulation of T cell autoreactivity by anomalous expression of NKG2D and its MIC ligands in rheumatoid arthritis. Proc. Natl. Acad. Sci. USA. 100, 9452–9457. https://doi.org/10.1073/pnas.1632807100.

Groh, V., Rhinehart, R., Randolph-Habecker, J., Topp, M.S., Riddell, S.R., and Spies, T. (2001). Costimulation of CD8alphabeta T cells by NKG2D via engagement by MIC induced on virus-infected cells. Nat. Immunol. 2, 255–260. https://doi.org/10.1038/85321.

Groh, V., Wu, J., Yee, C., and Spies, T. (2002). Tumour-derived soluble MIC ligands impair expression of NKG2D and T-cell activation. Nature 419, 734–738. https://doi.org/10.1038/nature01112.

Haapaniemi, E.M., Kaustio, M., Rajala, H.L.M., Van Adrichem, A.J., Kainulainen, L., Glumoff, V., Doffinger, R., Kuusanmäki, H., Heiskanen-Kosma, T., Trotta, L., et al. (2015). Autoimmunity, hypogammaglobulinemia, lymphoproliferation, and mycobacterial disease in patients with activating mutations in STAT3. Blood 125, 639–648. https://doi.org/10.1182/blood-2014-04-570101.

Huang, M., Wang, J., Torre, E., Dueck, H., Shaffer, S., Bonasio, R., Murray, J.I., Raj, A., Li, M., and Zhang, N.R. (2018). SAVER: gene expression recovery for single-cell RNA sequencing. Nat. Methods 15, 539–542. https://doi.org/10.1038/s41592-018-0033-z.

Hüe, S., Mention, J.J., Monteiro, R.C., Zhang, S., Cellier, C., Schmitz, J., Verkarre, V., Fodil, N., Bahram, S., Cerf-Bensussan, N., and Caillat-Zucman, S. (2004). A direct role for NKG2D/MICA interaction in villous atrophy during celiac disease. Immunity 21, 367–377. https://doi.org/10.1016/j.immuni.2004.06.018.

Ishida, F., Matsuda, K., Sekiguchi, N., Makishima, H., Taira, C., Momose, K., Nishina, S., Senoo, N., Sakai, H., Ito, T., and Kwong, Y.L. (2014). STAT3 gene mutations and their association with pure red cell aplasia in large granular lymphocyte leukemia. Cancer Sci. 105, 342–346. https://doi.org/10.1111/cas.12341.

Ives, M.L., Ma, C.S., Palendira, U., Chan, A., Bustamante, J., Boisson-Dupuis, S., Arkwright, P.D., Engelhard, D., Averbuch, D., Magdorf, K., et al. (2013). Signal transducer and activator of transcription 3 (STAT3) mutations underlying autosomal dominant hyper-IgE syndrome impair human CD8(+) T-cell memory formation and function. J. Allergy Clin. Immunol. 132, 400–411.e9. https://doi.org/10.1016/j.jaci.2013.05.029.

Jabri, B., and Abadie, V. (2015). IL-15 functions as a danger signal to regulate tissue-resident T cells and tissue destruction. Nat. Rev. Immunol. 15, 771–783. https://doi.org/10.1038/nri3919.

Jamieson, A.M., Diefenbach, A., Mcmahon, C.W., Xiong, N., Carlyle, J.R., and Raulet, D.H. (2002). The role of the NKG2D immunoreceptor in immune cell activation and natural killing. Immunity 17, 19–29.

Jerez, A., Clemente, M.J., Makishima, H., Koskela, H., Leblanc, F., Peng Ng, K., Olson, T., Przychodzen, B., Afable, M., Gomez-Segui, I., et al. (2012). STAT3 mutations unify the pathogenesis of chronic lymphoproliferative disorders of NK cells and T-cell large granular lymphocyte leukemia. Blood 120, 3048–3057. https://doi.org/10.1182/blood-2012-06-435297.

Jerez, A., Clemente, M.J., Makishima, H., Rajala, H., Gómez-Seguí, I., Olson, T., Mcgraw, K., Przychodzen, B., Kulasekararaj, A., Afable, M., et al. (2013). STAT3 mutations indicate the presence of subclinical T-cell clones in a subset of aplastic anemia and myelodysplastic syndrome patients. Blood 122, 2453–2459. https://doi.org/10.1182/blood-2013-04-494930.

Kaech, S.M., Hemby, S., Kersh, E., and Ahmed, R. (2002). Molecular and functional profiling of memory CD8 T cell differentiation. Cell 111, 837–851. https://doi.org/10.1016/s0092-8674(02)01139-x.

Karimi, M., Cao, T.M., Baker, J.A., Verneris, M.R., Soares, L., and Negrin, R.S. (2005). Silencing human NKG2D, DAP10, and DAP12 reduces cytotoxicity of activated CD8+ T cells and NK cells. J. Immunol. 175, 7819–7828.

Kawakami, T., Sekiguchi, N., Kobayashi, J., Imi, T., Matsuda, K., Yamane, T., Nishina, S., Senoo, Y., Sakai, H., Ito, T., et al. (2018). Frequent STAT3 mutations in CD8(+) T cells from patients with pure red cell aplasia. Blood Adv. 2, 2704–2712. https://doi.org/10.1182/bloodadvances.2018022723.

Kerr, C.M., Clemente, M.J., Chomczynski, P.W., Przychodzen, B., Nagata, Y., Adema, V., Visconte, V., Lichtin, A.E., Mustjoki, S., Radivoyevitch, T., et al. (2019). Subclonal STAT3 mutations solidify clonal dominance. Blood Adv. 3, 917–921. https://doi.org/10.1182/bloodadvances.2018027862.

Kim, D., Myllymäki, M., Kankainen, M., Jarvinen, T., Park, G., Bruhn, R., Murphy, E.L., and Mustjoki, S. (2021). Somatic STAT3 mutations in CD8+ T cells of healthy blood donors carrying human T-cell leukemia virus type 2. Haematologica 107, 550–554. https://doi.org/10.3324/haematol.2021.279140.

Kim, J., Chang, D.Y., Lee, H.W., Lee, H., Kim, J.H., Sung, P.S., Kim, K.H., Hong, S.H., Kang, W., Lee, J., et al. (2018). Innate-like Cytotoxic Function of Bystander-Activated CD8(+) T Cells Is Associated with Liver Injury in Acute Hepatitis A. Immunity 48, 161–173.e5. https://doi.org/10.1016/j.immuni.2017.11.025.

Korsunsky, I., Millard, N., Fan, J., Slowikowski, K., Zhang, F., Wei, K., Baglaenko, Y., Brenner, M., Loh, P.R., and Raychaudhuri, S. (2019). Fast, sensitive and accurate integration of single-cell data with harmony. Nat. Methods 16, 1289–1296. https://doi.org/10.1038/s41592-019-0619-0.

Koskela, H.L.M., Eldfors, S., Ellonen, P., Van Adrichem, A.J., Kuusanmäki, H., Andersson, E.I., Lagström, S., Clemente, M.J., Olson, T., Jalkanen, S.E., et al. (2012). Somatic STAT3 mutations in large granular lymphocytic leukemia. N. Engl. J. Med. 366, 1905–1913. https://doi.org/10.1056/NEJMoa1114885.

Ku, C.C., Kappler, J., and Marrack, P. (2001). The growth of the very large CD8+ T cell clones in older mice is controlled by cytokines. J. Immunol. 166, 2186–2193. https://doi.org/10.4049/jimmunol.166.4.2186.

Ku, C.C., Murakami, M., Sakamoto, A., Kappler, J., and Marrack, P. (2000). Control of homeostasis of CD8+ memory T cells by opposing cytokines. Science 288, 675–678. https://doi.org/10.1126/science.288.5466.675.

Lamy, T., Moignet, A., and Loughran, T.P., Jr. (2017). LGL leukemia: from pathogenesis to treatment. Blood 129, 1082–1094. https://doi.org/10.1182/blood-2016-08-692590.

Lu, C., Klement, J.D., Ibrahim, M.L., Xiao, W., Redd, P.S., Nayak-Kapoor, A., Zhou, G., and Liu, K. (2019). Type I interferon suppresses tumor growth through activating the STAT3-granzyme B pathway in tumor-infiltrating cytotoxic T lymphocytes. J. Immunother. Cancer 7, 157. https://doi.org/10.1186/s40425-019-0635-8.

Lun, A.T.L., Riesenfeld, S., Andrews, T., Dao, T.P., Gomes, T.; participants in the 1st Human Cell Atlas Jamboree, and Marioni, J.C. (2019). EmptyDrops: distinguishing cells from empty droplets in droplet-based single-cell RNA sequencing data. Genome Biol. 20, 63. https://doi.org/10.1186/s13059-019-1662-y.

Magoč, T., and Salzberg, S.L. (2011). FLASH: fast length adjustment of short reads to improve genome assemblies. Bioinformatics 27, 2957–2963. https://doi.org/10.1093/bioinformatics/btr507.

Markiewicz, M.A., Wise, E.L., Buchwald, Z.S., Pinto, A.K., Zafirova, B., Polic, B., and Shaw, A.S. (2012). RAE1epsilon ligand expressed on pancreatic islets recruits NKG2D receptor-expressing cytotoxic T cells independent of T cell receptor recognition. Immunity 36, 132–141. https://doi.org/10.1016/j.immuni.2011.11.014.

Mcinnes, I.B., Al-Mughales, J., Field, M., Leung, B.P., Huang, F.P., Dixon, R., Sturrock, R.D., Wilkinson, P.C., and Liew, F.Y. (1996). The role of interleukin-15 in T-cell migration and activation in rheumatoid arthritis. Nat. Med. 2, 175–182.

Meresse, B., Chen, Z., Ciszewski, C., Tretiakova, M., Bhagat, G., Krausz, T.N., Raulet, D.H., Lanier, L.L., Groh, V., Spies, T., et al. (2004). Coordinated induction by IL15 of a TCR-independent NKG2D signaling pathway converts CTL into lymphokine-activated killer cells in celiac disease. Immunity 21, 357–366. https://doi.org/10.1016/j.immuni.2004.06.020.

Milner, J.D., Vogel, T.P., Forbes, L., Ma, C.A., Stray-Pedersen, A., Niemela, J.E., Lyons, J.J., Engelhardt, K.R., Zhang, Y., Topcagic, N., et al. (2015). Early-onset lymphoproliferation and autoimmunity caused by germline STAT3 gain-of-function mutations. Blood 125, 591–599. https://doi.org/10.1182/blood-2014-09-602763.

Morgan, E.A., Lee, M.N., Deangelo, D.J., Steensma, D.P., Stone, R.M., Kuo, F.C., Aster, J.C., Gibson, C.J., and Lindsley, R.C. (2017). Systematic STAT3 sequencing in patients with unexplained cytopenias identifies unsuspected large granular lymphocytic leukemia. Blood Adv. 1, 1786–1789. https://doi.org/10.1182/bloodadvances.2017011197.

Morley, J.K., Batliwalla, F.M., Hingorani, R., and Gregersen, P.K. (1995). Oligoclonal CD8+ T cells are preferentially expanded in the CD57+ subset. J. Immunol. 154, 6182–6190.

Ng, S.S., De Labastida Rivera, F., Yan, J., Corvino, D., Das, I., Zhang, P., Kuns, R., Chauhan, S.B., Hou, J., Li, X.Y., et al. (2020). The NK cell granule protein NKG7 regulates cytotoxic granule exocytosis and inflammation. Nat. Immunol. 21, 1205–1218. https://doi.org/10.1038/s41590-020-0758-6.

Ogasawara, K., Hamerman, J.A., Ehrlich, L.R., Bour-Jordan, H., Santamaria, P., Bluestone, J.A., and Lanier, L.L. (2004). NKG2D blockade prevents autoimmune diabetes in NOD mice. Immunity 20, 757–767. https://doi.org/10.1016/j.immuni.2004.05.008.

Ogawa, K., Tanaka, K., Ishii, A., Nakamura, Y., Kondo, S., Sugamura, K., Takano, S., Nakamura, M., and Nagata, K. (2001). A novel serum protein that is selectively produced by cytotoxic lymphocytes. J. Immunol. 166, 6404–6412. https://doi.org/10.4049/jimmunol.166.10.6404.

O'shea, J.J., Holland, S.M., and Staudt, L.M. (2013). JAKs and STATs in immunity, immunodeficiency, and cancer. N. Engl. J. Med. 368, 161–170. https://doi.org/10.1056/NEJMra1202117.

Park, Y.P., Choi, S.C., Kiesler, P., Gil-Krzewska, A., Borrego, F., Weck, J., Krzewski, K., and Coligan, J.E. (2011). Complex regulation of human NKG2D-DAP10 cell surface expression: opposing roles of the gammac cytokines and TGF-beta1. Blood 118, 3019–3027. https://doi.org/10.1182/blood-2011-04-346825.

Picelli, S., Faridani, O.R., Björklund, A.K., Winberg, G., Sagasser, S., and Sandberg, R. (2014). Full-length RNA-seq from single cells using Smartseq2. Nat. Protoc. 9, 171–181. https://doi.org/10.1038/nprot.2014.006.

Posnett, D.N., Sinha, R., Kabak, S., and Russo, C. (1994). Clonal populations of T cells in normal elderly humans: the T cell equivalent to "benign monoclonal gammapathy. J. Exp. Med. 179, 609–618. https://doi.org/10.1084/jem.179.2.609.

Qiu, Z.Y., Fan, L., Wang, L., Qiao, C., Wu, Y.J., Zhou, J.F., Xu, W., and Li, J.Y. (2013). STAT3 mutations are frequent in T-cell large granular lymphocytic leukemia with pure red cell aplasia. J. Hematol. Oncol. 6, 82. https://doi.org/10.1186/1756-8722-6-82.

Rajala, H.L.M., Olson, T., Clemente, M.J., Lagström, S., Ellonen, P., Lundan, T., Hamm, D.E., Zaman, S.A.U., Lopez Marti, J.M., Andersson, E.I., et al. (2015). The analysis of clonal diversity and therapy responses using STAT3 mutations as a molecular marker in large granular lymphocytic leukemia. Haematologica 100, 91–99. https://doi.org/10.3324/haematol.2014.113142.

Raulet, D.H., Gasser, S., Gowen, B.G., Deng, W., and Jung, H. (2013). Regulation of ligands for the NKG2D activating receptor. Annu. Rev. Immunol. 31, 413–441. https://doi.org/10.1146/annurev-immunol-032712-095951.

Ritchie, M.E., Phipson, B., Wu, D., Hu, Y., Law, C.W., Shi, W., and Smyth, G.K. (2015). limma powers differential expression analyses for RNA-sequencing and microarray studies. Nucleic Acids Res. 43, e47. https://doi.org/10.1093/nar/gkv007.

Roberts, A.I., Lee, L., Schwarz, E., Groh, V., Spies, T., Ebert, E.C., and Jabri, B. (2001). NKG2D receptors induced by IL-15 costimulate CD28-negative effector CTL in the tissue microenvironment. J. Immunol. 167, 5527–5530.

Satija, R., Farrell, J.A., Gennert, D., Schier, A.F., and Regev, A. (2015). Spatial reconstruction of single-cell gene expression data. Nat. Biotechnol. 33, 495–502. https://doi.org/10.1038/nbt.3192.

Savola, P., Brück, O., Olson, T., Kelkka, T., Kauppi, M.J., Kovanen, P.E., Kytölä, S., Sokka-Isler, T., Loughran, T.P., Leirisalo-Repo, M., and Mustjoki, S. (2018). Somatic STAT3 mutations in Felty syndrome: an implication for a common pathogenesis with large granular lymphocyte leukemia. Haematologica 103, 304–312. https://doi.org/10.3324/haematol.2017.175729.

Shi, M., He, R., Feldman, A.L., Viswanatha, D.S., Jevremovic, D., Chen, D., and Morice, W.G. (2018). STAT3 mutation and its clinical and histopathologic correlation in T-cell large granular lymphocytic leukemia. Hum. Pathol. 73, 74–81. https://doi.org/10.1016/j.humpath.2017.12.014.

Siegel, A.M., Heimall, J., Freeman, A.F., Hsu, A.P., Brittain, E., Brenchley, J.M., Douek, D.C., Fahle, G.H., Cohen, J.I., Holland, S.M., and Milner, J.D. (2011). A critical role for STAT3 transcription factor signaling in the development and maintenance of human T cell memory. Immunity 35, 806–818. https://doi.org/10.1016/j.immuni.2011.09.016.

Singh, M., Al-Eryani, G., Carswell, S., Ferguson, J.M., Blackburn, J., Barton, K., Roden, D., Luciani, F., Giang Phan, T., Junankar, S., et al. (2019). High-throughput targeted long-read single cell sequencing reveals the clonal and transcriptional landscape of lymphocytes. Nat. Commun. 10, 3120. https://doi.org/10.1038/s41467-019-11049-4.

Smith, L.K., Boukhaled, G.M., Condotta, S.A., Mazouz, S., Guthmiller, J.J., Vijay, R., Butler, N.S., Bruneau, J., Shoukry, N.H., Krawczyk, C.M., and Richer, M.J. (2018). Interleukin-10 directly inhibits CD8(+) T cell function by enhancing N-glycan branching to decrease antigen sensitivity. Immunity 48, 299–312.e5. https://doi.org/10.1016/j.immuni.2018.01.006.

Soderquist, C.R., Lewis, S.K., Gru, A.A., Vlad, G., Williams, E.S., Hsiao, S., Mansukhani, M.M., Park, D.C., Bacchi, C.E., Alobeid, B., et al. (2021). Immunophenotypic spectrum and genomic landscape of refractory celiac disease Type II. Am. J. Surg. Pathol. 45, 905–916. https://doi.org/10.1097/PAS.0000000000001658.

Stoeckius, M., Hafemeister, C., Stephenson, W., Houck-Loomis, B., Chattopadhyay, P.K., Swerdlow, H., Satija, R., and Smibert, P. (2017). Simultaneous epitope and transcriptome measurement in single cells. Nat. Methods 14, 865–868. https://doi.org/10.1038/nmeth.4380.

Stonier, S.W., Ma, L.J., Castillo, E.F., and Schluns, K.S. (2008). Dendritic cells drive memory CD8 T-cell homeostasis via IL-15 transpresentation. Blood 112, 4546–4554. https://doi.org/10.1182/blood-2008-05-156307.

Sutherland, C.L., Chalupny, N.J., and Cosman, D. (2001). The UL16-binding proteins, a novel family of MHC class I-related ligands for NKG2D, activate natural killer cell functions. Immunol. Rev. 181, 185–192. https://doi.org/10.1034/j.1600-065x.2001.1810115.x.

Valori, M., Jansson, L., and Tienari, P.J. (2021). CD8+ cell somatic mutations in multiple sclerosis patients and controls-Enrichment of mutations in STAT3 and other genes implicated in hematological malignancies. PLoS One 16, e0261002. https://doi.org/10.1371/journal.pone.0261002.

Vander Heiden, J.A., Yaari, G., Uduman, M., Stern, J.N.H., O'connor, K.C., Hafler, D.A., Vigneault, F., and Kleinstein, S.H. (2014). pRESTO: a toolkit for processing high-throughput sequencing raw reads of lymphocyte receptor repertoires. Bioinformatics 30, 1930–1932. https://doi.org/10.1093/bioinformatics/btu138.

Verneris, M.R., Karimi, M., Karami, M., Baker, J., Jayaswal, A., and Negrin, R.S. (2004). Role of NKG2D signaling in the cytotoxicity of activated and expanded CD8+ T cells. Blood 103, 3065–3072. https://doi.org/10.1182/blood-2003-06-2125.

Voshol, H., Van Zuylen, C.W., Orberger, G., Vliegenthart, J.F., and Schachner, M. (1996). Structure of the HNK-1 carbohydrate epitope on bovine peripheral myelin glycoprotein P0. J. Biol. Chem. 271, 22957–22960. https://doi.org/10.1074/jbc.271.38.22957.

Wakabayashi, Y., Mao, J.H., Brown, K., Girardi, M., and Balmain, A. (2007). Promotion of Hras-induced squamous carcinomas by a polymorphic variant of the Patched gene in FVB mice. Nature 445, 761–765. https://doi.org/10.1038/nature05489.

Waldmann, T.A., Miljkovic, M.D., and Conlon, K.C. (2020). Interleukin-15 (dys) regulation of lymphoid homeostasis: Implications for therapy of autoimmunity and cancer. J. Exp. Med. 217, e20191062. https://doi.org/10.1084/jem.20191062.

Warshauer, J.T., Belk, J.A., Chan, A.Y., Wang, J., Gupta, A.R., Shi, Q., Skartsis, N., Peng, Y., Phipps, J.D., Acenas, D., et al. (2021). A human mutation in STAT3 promotes type 1 diabetes through a defect in CD8+ T cell tolerance. J. Exp. Med. 218, e20210759. https://doi.org/10.1084/jem.20210759.

Wu, J., Song, Y., Bakker, A.B., Bauer, S., Spies, T., Lanier, L.L., and Phillips, J.H. (1999). An activating immunoreceptor complex formed by NKG2D and DAP10. Science 285, 730–732.

Xiao, Z., Mescher, M.F., and Jameson, S.C. (2007). Detuning CD8 T cells: down-regulation of CD8 expression, tetramer binding, and response during CTL activation. J. Exp. Med. 204, 2667–2677. https://doi.org/10.1084/jem.20062376.

Xing, L., Dai, Z., Jabbari, A., Cerise, J.E., Higgins, C.A., Gong, W., De Jong, A., Harel, S., Destefano, G.M., Rothman, L., et al. (2014). Alopecia areata is driven by cytotoxic T lymphocytes and is reversed by JAK inhibition. Nat. Med. 20, 1043–1049. https://doi.org/10.1038/nm.3645.

Yang, H., Wang, H., and Jaenisch, R. (2014). Generating genetically modified mice using CRISPR/Cas-mediated genome engineering. Nat. Protoc. 9, 1956–1968. https://doi.org/10.1038/nprot.2014.134.

Yang, J., Liao, X., Agarwal, M.K., Barnes, L., Auron, P.E., and Stark, G.R. (2007). Unphosphorylated STAT3 accumulates in response to IL-6 and activates transcription by binding to NFkappaB. Genes Dev. *21*, 1396–1408. https://doi.org/10.1101/gad.1553707.

Ye, J., Ma, N., Madden, T.L., and Ostell, J.M. (2013). IgBLAST: an immunoglobulin variable domain sequence analysis tool. Nucleic Acids Res. *41*, W34–W40. https://doi.org/10.1093/nar/gkt382.

Zhang, R., Shah, M.V., and Loughran, T.P., Jr. (2010). The root of many evils: indolent large granular lymphocyte leukaemia and associated disorders. Hematol. Oncol. *28*, 105–117. https://doi.org/10.1002/hon.917.

Zhang, X., Sun, S., Hwang, I., Tough, D.F., and Sprent, J. (1998). Potent and selective stimulation of memory-phenotype CD8+ T cells in vivo by IL-15. Immunity *8*, 591–599. https://doi.org/10.1016/s1074-7613(00)80564-6.

Zhu, S., Phatarpekar, P.V., Denman, C.J., Senyukov, V.V., Somanchi, S.S., Nguyen-Jackson, H.T., Mace, E.M., Freeman, A.F., Watowich, S.S., Orange, J.S., et al. (2014). Transcription of the activating receptor NKG2D in natural killer cells is regulated by STAT3 tyrosine phosphorylation. Blood *124*, 403–411. https://doi.org/10.1182/blood-2013-05-499707.

STAR★METHODS

KEY RESOURCES TABLE

REAGENT or RESOURCE	SOURCE	IDENTIFIER
Antibodies		
7AAD	Invitrogen	Cat# A1310
Rat IgG2b Anti-Mouse CD3 FITC; Clone 17A2	BioLegend	Cat# 100204; RRID: AB_312660
Rat IgG2b Anti-Mouse CD3 PerCP Cy5.5; Clone 17A2	BioLegend	Cat# 100217; RRID: AB_1595597
Rat IgG2b Anti-Mouse CD4 BV786; Clone GK1.5	BD Biosciences	Cat# 563331; RRID: AB_2738140
Rat IgG2b Anti-Mouse CD4 BUV737; Clone SK3	BD Biosciences	Cat# 564306; RRID: AB_2713927
Rat IgG2a Anti-Mouse CD5 APC; Clone 53-7.3	Thermo Fischer	Cat 17-0051-81; RRID: AB_563796
Rat IgG2a Anti-Mouse CD8 BUV395; Clone 53-6.7	BD Biosciences	Cat# 563786; RRID: AB_2732919
Rat IgG2a Anti-Mouse CD8 APC Cy7; Clone 53-6.7	BD Biosciences	Cat# 557654; RRID: AB_396769
Rat IgG2b Anti-Mouse CD11b FITC; Clone M1/70	BD Biosciences	Cat# 557396; RRID: AB_396679
Rat IgG2b Anti-Mouse CD11b PE; Clone M1/70	BioLegend	Cat# 101208; RRID: AB_312791
Armenian Hamster IgG Anti-Mouse CD11c PerCP/Cy5.5; Clone N418	eBioscience	Cat 45-0114-82; RRID: AB_1548654
Rat IgG2a Anti-Mouse CD19 BV510; Clone 6D5	BioLegend	Cat# 115546; RRID: AB_2562137
Rat IgG2a Anti-Mouse CD19 BV605; Clone 6D5	BioLegend	Cat# 115539; RRID: AB_11203538
Rat IgG2b Anti-Mouse CD24 Pacific Blue; Clone M1/69	BioLegend	Cat# 101820; RRID: AB_572011
Rat IgG1 Anti-Mouse CD25 PerCP Cy5.5; Clone PC61	BioLegend	Cat# 102030; RRID: AB_893288
Rat IgM Anti-Mouse CD25 PE; Clone 7D4	BD Biosciences	Cat# 558642; RRID: AB_1645250
Rat IgG1 Anti-Mouse CD25 APC; Clone PC61	BD Biosciences	Cat# 557192; RRID: AB_398623
Armenian Hamster IgG Anti-Mouse CD27 PE Cy7; Clone LG.3A10	BioLegend	Cat 124216; RRID: AB_10639726
Mouse IgG2b Anti-Mouse CD28 FITC; Clone E18	BioLegend	Cat# 122007; RRID: AB_604062
Rat IgG2a Anti-Mouse CD38 BV421; Clone Ab90	BD Biosciences	Cat# 562768; RRID: AB_2737781
Rat IgG2b Anti-Mouse CD44 BV605; Clone IM7	BD Biosciences	Cat# 563058; RRID: AB_2737979
Rat IgG2b Anti-Mouse CD44 Pacific Blue; Clone IM7	BioLegend	Cat# 103020; RRID: AB_493683
Rat IgG2b Anti-Mouse CD44 FITC; Clone IM7	BD Biosciences	Cat# 553133; RRID: AB_2076224
Mouse IgG2a Anti-Mouse CD45.1 BUV737; Clone A20	BD Biosciences	Cat# 564574; RRID: AB_2738850
Mouse IgG2a Anti-Mouse CD45.1 APC Cy7; Clone A20	Biolegend	Cat# 110716; RRID: AB_313505
Mouse IgG2a Anti-Mouse CD45.1 PerCP Cy5.5; Clone A20	Biolegend	Cat# 110728; RRID: AB_893346
Mouse IgG2a Anti-Mouse CD45.2 PE Cy7; Clone 104	BD Biosciences	Cat# 560696; RRID: AB_1727494
Mouse IgG2a Anti-Mouse CD45.2 BUV395; Clone 104	BD Biosciences	Cat# 564616; RRID: AB_2738867
Mouse IgG2a Anti-Mouse CD45.2 APC Cy7; Clone 104	BioLegend	Cat# 109824; RRID: AB_830789
Rat IgG2a Anti-Mouse CD45R/B220 BUV737; Clone RA3-6B2	BD Biosciences	Cat# 564449; RRID: AB_2738813
Rat IgG2a Anti-Mouse CD62L BV605; Clone MEL-14	BioLegend	Cat# 104438; RRID: AB_2563058
Rat IgG2a Anti-Mouse CD62L PerCP Cy5.5; Clone MEL-14	BD Biosciences	Cat# 560513; RRID: AB_10611578
Armenian Hamster IgG Anti-Mouse CD69 PE; Clone H1.2F3	BioLegend	Cat# 104508; RRID: AB_313111
Armenian Hamster IgG2 Anti-Mouse CD95 PE Cy7; Clone Jo2	BD Biosciences	Cat# 557653; RRID: AB_396768
Rat IgG2b Anti-Mouse CD126 (IL-6Ra) Biotin; Clone D7715A7	BioLegend	Cat# 115803; RRID: AB_313674
Rat IgG2b Anti-Mouse CD126 (IL-6Ra) PE; Clone D7715A7	BioLegend	Cat# 115806; RRID: AB_313677
Rat IgG2a Anti-Mouse CD127 (IL-7Ra) PE Cy7; Clone eBR2a	Thermo Fischer	Cat# 25-1271-82; RRID: AB_469649
Rat IgG2b Anti-Mouse CD132 (U_C) Biotin; Clone 10H5	Thermo Fischer	Cat# 13-1321-82; RRID: AB_10736474
Armenian Hamster IgG Anti-Mouse CD152 (CTLA-4) APC; Clone UC10-4B9	Thermo Fischer	Cat# 17-1522-80; RRID: AB_2016700
Armenian Hamster IgG Anti-Mouse CD196 (CCR6) PE; Clone 29-2L17	BioLegend	Cat# 129804; RRID: AB_1279137

(Continued on next page)

Continued

REAGENT or RESOURCE	SOURCE	IDENTIFIER
Armenian Hamster IgG Anti-Mouse CD196 (CCR6) PE Cy7; Clone 29-2L17	BioLegend	Cat# 129816; RRID: AB_2072798
Rat IgG1 Anti-Mouse CD210 (IL-10R) PE; Clone 1b1.3a	BioLegend	Cat# 112705; RRID: AB_313518
Rat IgG2a Anti-Mouse CD215 (IL-15Ra) PE; Clone 6B4C88	BioLegend	Cat# 153504; RRID: AB_2721342
Rat IgG2a Anti-Mouse CD215 (IL-15Ra) APC; Clone 6B4C88	BioLegend	Cat# 153506; RRID: AB_2728209
Armenian Hamster IgG Anti-Mouse CD278 (ICOS) PE; Clone C398.4A	Thermo Fischer	Cat# 12-9949-81; RRID: AB_466277
Armenian Hamster IgG Anti-Mouse CD278 (ICOS) APC/Cy7; Clone C398.4A	BioLegend	Cat# 313529; RRID: AB_2566127
Armenian Hamster IgG Anti-Mouse CD278 (ICOS) BV711; Clone C398.4A	BioLegend	Cat# 313548; RRID: AB_2734289
Armenian Hamster IgG Anti-Mouse CD279 (PD1) PE Cy7; Clone J43	Thermo Fischer	Cat# 25-9985-82; RRID: AB_10853805
Armenian Hamster IgG2 Anti-Mouse CD279 (PD1) PE; Clone J43	BD Biosciences	Cat# 551892; RRID: AB_394284
Rat IgG2a Anti-Mouse CD360 (IL-21R) Biotin; Clone eBio4A9	Thermo Fischer	Cat# 13-1219-81; RRID: AB_466573
Mouse IgG1 Anti-Mouse Bcl-2 PE Cy7; Clone BCL/10C4	BioLegend	Cat# 633511; RRID: AB_2565246
Mouse IgG2a Anti-Mouse CX3CR1 BV785; Clone SA011F11	BioLegend	Cat# 149029; RRID: AB_2565938
Rat IgG2b Anti-Mouse FoxP3 AF488; Clone MF-14	BioLegend	Cat# 126406; RRID: AB_1089113
Rat IgG2a Anti-Mouse FoxP3 PE/Cy7; Clone FJK-16s	Thermo Fischer	Cat# 25-5773-82; RRID: AB_891552
Rat IgG2a Anti-Mouse FoxP3 eF450; Clone FJK-16s	Thermo Fischer	Cat# 48-5773-80; RRID: AB_1518812
Syrian Hamster IgG2 Anti-Mouse KLRG1 BV786; Clone 2F1	BD Biosciences	Cat# 565477; RRID: AB_2739256
Rat IgM Anti-Mouse Ly-6C Biotin; Clone AL-21	BD Biosciences	Cat# 557359; RRID: AB_396663
Rat IgG2a Anti-Mouse Ly-6G PE Cy7; Clone 1A8	BD Biosciences	Cat# 560601; RRID: AB_1727562
Rat IgG2a Anti-Mouse ULBP1/MULT1 PE; Clone 237104	R&D Systems	Cat# FAB2588P; RRID: AB_10973344
Mouse IgG2a Anti-Mouse NK1.1 BV510; Clone PK136	BioLegend	Cat# 108738; RRID: AB_2562217
Rat IgG2a Anti-Mouse NKG2A/C/E BUV395; Clone 20d5	BD Biosciences	Cat# 740276; RRID: AB_465305
Rat IgG1 Anti-Mouse NKG2D APC; Clone CX5	BioLegend	Cat# 130212; RRID: AB_1236372
Rat IgG1 Anti-Mouse NKG2D PE; Clone CX5	BioLegend	Cat# 130208; RRID: AB_1227712
Streptavidin BV605	BioLegend	Cat# 405229
Mouse IgG1 Anti- Tbet APC; Clone 4B10	BioLegend	Cat# 644814; RRID: AB_10901173
Armenian Hamster IgG Anti-Mouse TCRβ APC Cy7; Clone H57-597	BioLegend	Cat# 109220; RRID: AB_893624
Armenian Hamster IgG Anti-Mouse TCRβ PerCP Cy5.5; Clone H57-597	BioLegend	Cat# 109227; RRID: AB_1575176
Mouse IgG1 Anti-Human CD25 FITC; Clone 2A3	BD Biosciences	Cat# 347643; RRID: AB_400334
Mouse IgM Anti-Human CD57 FITC; Clone NK-1	BD Pharmingen	Cat# 555619; RRID: AB_395986
Mouse IgG1 Anti-Human CD314 (NKG2D) PerCP eF710; Clone 1D11	eBioScience	Cat# 46-5878-42; RRID: AB_2573787
Mouse IgG1 Anti-Human CD28 APC; Clone CD28.2	eBioScience	Cat# 17-0289-42; RRID: AB_10597439
Rat IgG2b Anti-Human CX3CR1 APC; Clone 2A9-1	BioLegend	Cat# 341610; RRID: AB_2087424
Armenian Hamster IgG Anti-Human CD278 (ICOS) Biotin; Clone C398.4A	eBioScience	Cat# 13-9949-82; RRID: AB_467006
Mouse IgG2b Anti-Human CD44 Biotin; Clone G44-26	BD Pharmingen	Cat# 555477; RRID: AB_395869
Mouse IgG1 Anti-Human CD3 BV421; Clone UCHT1	BD Horizon	Cat# 562426; RRID: AB_11152082

Continued

REAGENT or RESOURCE	SOURCE	IDENTIFIER
Mouse IgG2b Anti-Human CD45RA BV605; Clone HI100	BD Horizon	Cat# 562886; RRID: AB_2737865
Mouse IgG1 Anti-Human CD127 BV650; Clone A019D5	BioLegend	Cat# 351326; RRID: AB_2562095
Mouse IgG1 Anti-Human CD69 BV711; Clone FN50	BD Horizon	Cat# 563836; RRID: AB_2738443
Mouse IgG2a Anti-Human CD62L BV711; Clone SK11	BD Horizon	Cat# 565040; RRID: AB_2869642
Mouse IgG1 Anti-Human CD27 BV786; Clone L128	BD Horizon	Cat# 563327; RRID: AB_2744353
Mouse IgG1 Anti-Human CD38 PE; Clone HIT2	Invitrogen	Cat# MHCD3804; RRID: AB_10371762
Mouse IgG1 Anti-Human CD278 (ICOS) PE; Clone C398.4A	eBioscience	Cat# 12-9948-81; RRID: AB_10732348
Mouse IgG1 Anti-Human CD95 PE CF594; Clone DX2	BD Horizon	Cat# 562395; RRID: AB_11153666
Mouse IgG2a Anti-Human CD197 (CCR7) PE Cy7; Clone G043H7	BioLegend	Cat# 353226; RRID: AB_11126145
Mouse IgG1 Anti-Human CD8 BUV395; Clone RPA-T8	BD Biosciences	Cat# 563796; RRID: AB_2722501
Mouse IgG1 Anti-Human CD4 BUV737; Clone SK3	BD Horizon	Cat# 564305; RRID: AB_2713927
TotalSeq™-A0301 anti-mouse Hashtag 1 Antibody; Clones M1/42, 30-F11	BioLegend	Cat# 155801; RRID: AB_2750032
TotalSeq™-A0302 anti-mouse Hashtag 2 Antibody; Clones M1/42, 30-F11	BioLegend	Cat# 155803; RRID: AB_2750033
TotalSeq™-A0307 anti-mouse Hashtag 7 Antibody; Clones M1/42, 30-F11	BioLegend	Cat# 155813; RRID: AB_2750039
TotalSeq™-A0308 anti-mouse Hashtag 8 Antibody; Clones M1/42, 30-F11	BioLegend	Cat# 155815; RRID: AB_2750040
TotalSeq™-A0309 anti-mouse Hashtag 9 Antibody; Clones M1/42, 30-F11	BioLegend	Cat# 155817; RRID: AB_2750042
TotalSeq™-A0310 anti-mouse Hashtag 10 Antibody; Clones M1/42, 30-F11	BioLegend	Cat# 155819; RRID: AB_2750043
TotalSeq™-A0311 anti-mouse Hashtag 11 Antibody; Clones M1/42, 30-F11	BioLegend	Cat# 155821; RRID: AB_2750136
TotalSeq™-A0312 anti-mouse Hashtag 12 Antibody; Clones M1/42, 30-F11	BioLegend	Cat# 155823; RRID: AB_2750137
TotalSeq™-A0251 anti-human Hashtag 1 Antibody; Clones LNH-94; 2M2	BioLegend	Cat# 394601; RRID: AB_2750015
TotalSeq™-A0252 anti-human Hashtag 2 Antibody; Clones LNH-94; 2M2	BioLegend	Cat# 394603; RRID: AB_2750016
TotalSeq™-A0253 anti-human Hashtag 3 Antibody; Clones LNH-94; 2M2	BioLegend	Cat# 394605; RRID: AB_2750017
TotalSeq™-A0253 anti-human Hashtag 4 Antibody; Clones LNH-94; 2M2	BioLegend	Cat# 394607; RRID: AB_2750018
TotalSeq™-A0253 anti-human Hashtag 5 Antibody; Clones LNH-94; 2M2	BioLegend	Cat# 394609; RRID: AB_2750019
TotalSeq™-A0253 anti-human Hashtag 6 Antibody; Clones LNH-94; 2M2	BioLegend	Cat# 394611; RRID: AB_2750020
TotalSeq™-A0253 anti-human Hashtag 7 Antibody; Clones LNH-94; 2M2	BioLegend	Cat# 394613; RRID: AB_2750021
TotalSeq™-A0253 anti-human Hashtag 8 Antibody; Clones LNH-94; 2M2	BioLegend	Cat# 394615; RRID: AB_2750022
Armenian Hamster anti-mouse NKG2D; Clone HMG2D	BioXCell	Cat# BE0111; RRID: AB_10950118
Polyclonal Armenian Hamster IgG	BioXCell	Cat# BE0091; RRID: AB_1107773
Mouse anti-mouse CD122 (IL-2Rβ) ; Clone TM-β1	BioXCell	Cat# BE0298; RRID: AB_2687820

(Continued on next page)

Continued

REAGENT or RESOURCE	SOURCE	IDENTIFIER
Rat IgG2b anti-mouse IL-6R; Clone 15A7	BioXCell	Cat# BE0047; RRID: AB_1107588
Rat IgG2b isotype control, anti-keyhole limpet hemocyanin; Clone LTF-2	BioXCell	Cat# BE0090; RRID: AB_1107780
Rat IgG2a anti-mouse IL-21R; Clone 4A9	BioXCell	Cat# BE0258; RRID: AB_2687737
Rat IgG2a anti-mouse IL-7Rα; Clone A7R34	BioXCell	Cat# BE0065; RRID: AB_1107590
Rat IgG2a isotype control, anti-trinitrophenol; Clone 2A3	BioXCell	Cat# BE0089; RRID: AB_1107769
Biological samples		
Human whole blood samples	Multiple institutions	N/A
Chemicals, peptides, and recombinant proteins		
RPMI 1640 Medium	Life Technologies	Cat# 11875-119
Foetal Bovine Serum, NZ origin, heat inactivated	Assay Matrix	Cat# ASFBS-HI-NZ
Phosphate Buffered Saline	Internal Stores; Garvan Institute	Internal Stores; Garvan Institute
Collagenase D from *Clostridium histolyticum*	Sigma Aldrich	Cat# 11088866001
Dispase® II (neutral protease, grade II)	Sigma Aldrich	Cat# 4942078001
DNase I recombinant, RNase-free	Sigma Aldrich	Cat# 4716728001
Recombinant Mouse IL-15 (carrier-free)	BioLegend	Cat# 566302
eBioscience Foxp3 / Transcription Factor Staining Buffer Set	eBioscience	Cat# 00-5523-00
Critical commercial assays		
Chromium Next GEM Single Cell 3' Kit v3.1, 16 rxns	10X Genomics	Cat# PN-1000268
Deposited data		
Raw sequence data, from single-cell RNA sequencing of sorted mouse T cell populations	This paper	NCBI BioProject: PRJNA804580
Raw sequence data, from single-cell RNA, protein and TCR sequencing of sorted human T cell populations	This paper	NCBI BioProject: PRJNA804580
Experimental models: Organisms/strains		
Mouse: *Stat3*^{T716M}: *C57BL/6-Stat3T716M*	Garvan MEGA Facility; Prof. Robert Brink	N/A
Mouse: *Stat3*^{K658N}: *C57BL/6xFVB/J-Stat3K658N*	Garvan MEGA Facility; Prof. Robert Brink	N/A
Mouse: *Stat3*^{T716M} *Il10ra*$^{\Delta}$: *C57BL/6-Stat3T716M-Il10raΔ*	Garvan MEGA Facility; Prof. Robert Brink	N/A
Mouse: *Stat3*^{K658N} *Klrk1*$^{\Delta}$: *C57BL/6-Stat3K658N-Klrk1Δ*	Garvan MEGA Facility; Prof. Robert Brink	N/A
Mouse: *Stat3*^{K658N} *Cx3cr1*$^{\Delta}$: *C57BL/6-Stat3K658N-Cx3cr1Δ*	Garvan MEGA Facility; Prof. Robert Brink	N/A
Mouse: *Stat3*^{K658N} *Rag1*$^{\Delta}$: *C57BL/6-Stat3K658N-B6.129S7-Rag1^{tm1Mom}/JAusb*	Garvan MEGA Facility; Prof. Robert Brink	N/A
Mouse: C57BL/6J: C57BL/6 JAusb	The Jackson Laboratory	JAX: 000664
Mouse: CD45.1: B6.JSL-*Ptprc*^{a}*Pepc*^{b}/BoyJAusb	The Jackson Laboratory	JAX: 002014
Mouse: *Rag1*$^{KO/KO}$: B6.129S7-*Rag1*^{tm1Mom}/JAusb	The Jackson Laboratory	JAX: 002096

(Continued on next page)

Continued

REAGENT or RESOURCE	SOURCE	IDENTIFIER
Software and algorithms		
FLASH	(Magoc and Salzberg, 2011)	http://www.cbcb.umd.edu/software/flash
pRESTO	(Vander Heiden et al., 2014)	http://clip.med.yale.edu/presto
IgBLAST	(Ye et al., 2013)	http://www.ncbi.nlm.nih.gov/igblast/
Harmony	(Korsunsky et al., 2019)	https://github.com/immunogenomics/harmony
GraphPad Prims 9 – Version 9.0.0	GraphPad	https://www.graphpad.com
FlowJo V10 – Version 10.4.0	FlowJo	https://www.flowjo.com
EmptyDrops	(Lun et al., 2019)	https://github.com/MarioniLab/EmptyDrops2017
Limma	(Ritchie et al., 2015)	https://bioconductor.org/packages/release/bioc/html/limma.html
SAVER	(Huang et al., 2018)	https://github.com/mohuangx/SAVER
CellRanger	10X Genomics	Cell Ranger Single Cell v.2.0
Seurat	(Satija et al., 2015)	https://github.com/satijalab/seurat/

RESOURCE AVAILABILITY

Lead contact
Further information and requests for resources and reagents should be directed to and will be fulfilled by the Lead Contact, Christopher C. Goodnow (c.goodnow@garvan.org.au).

Materials availability
This study did not generate new unique reagents.

Data and code availability
- Single-cell RNA-seq and TCR mRNA deep sequencing data have been deposited in NCBI BioProject PRJNA804580. The accession number for these data is NCBI BioProject: PRJNA804580, as listed in the key resources table.
- Bioinformatic workflows used to analyze the data in this study are available upon request.
- Any additional information required to reanalyze the data reported in this paper is available from the lead contact upon request.

EXPERIMENTAL MODEL AND SUBJECT DETAILS

Human subjects
This study was approved by the respective ethics review boards of the participating institutes, including the Ethics committees of Sydney Local Health District RPAH Zone Human Research Ethics Committee and Research Governance Office, Royal Prince Alfred Hospital, Camperdown, NSW, Australia (Protocol X16-0210/LNR/16/RPAH/257); the South East Sydney Local Health District Human Research Ethics Committee, Prince of Wales/Sydney Children's Hospital, Randwick, NSW, Australia (Protocol HREC/11/POWH/152); the Helsinki University Hospital Ethics committee. Written informed consent for genetic investigations and immunological analyses, as well as publication of data, was obtained from each family.

Mouse handling, housing and husbandry
All mouse handling and experimental methods were performed in accordance with approved protocols of the Garvan Institute of Medical Research/St Vincent's Hospital Animal Ethics Committee. All mice were bred and maintained in specific pathogen-free conditions at Australian BioResources (ABR; Moss Vale, Australia) or at the Garvan Institute of Medical Research Biological Testing Facility (BTF). Within independent experiments, *Stat3* WT and mutant animals were sex- and age-matched. All experiments conformed to the current guidelines from the Australian Code of Practice for the Care and Use of Animals for Scientific Purposes. Mice were genotyped by the Garvan Molecular Genetics (GMG) facility at the Garvan Institute of Medical Research.

Mouse anatomy and histopathology
Detailed anatomical and histopathology analysis was performed as a commercial service, on over 40 organs from $Stat3^{T716M}$ WT (n = 3), HOM (n = 3), $Stat3^{K658N}$ WT (n = 5), HET (n = 1) and HOM (n = 5) mice, by the Phenomics Australia Histopathology and Slide Scanning Service (University of Melbourne, Australia).

CellPress
OPEN ACCESS

Mouse *strains*

*Stat3^T716M^*, *Stat3^K658N^*, *Il10ra^KO^*, *Klrk1^KO^* and *Cx3cr1^KO^* mice were produced by CRISPR/Cas9 gene targeting in mouse embryos, following established molecular and animal husbandry techniques (Yang et al., 2014). Target gene-specific single guide RNAs (sgRNA; 15 ng/μl) were microinjected into the nucleus and cytoplasm of mouse zygotes, together with polyadenylated *S. pyogenes Cas9* mRNA (30 ng/μl) and a gene-specific 150 base single-stranded, deoxy-oligonucleotide homologous recombination substrate (15 ng/μl). Injections were performed into C57BL/6 zygotes for each of these strains but the *Stat3^K658N^* strain, where injections were performed into C57BL/6J x FVB/N F1 zygotes. Founder mice HET for alleles successfully modified by homologous recombination were back-crossed with syngeneic partners and then inter-crossed to establish the *Stat3^T716M^* or *Stat3^K658N^* mouse lines.

For *Stat3^T716M^*, the sgRNA was produced based on a target site in exon 23 (CAGGTCAATGGTATTGCTGC*AGG* = T716M, PAM italicised and underlined) of *Stat3*. The deoxy-oligonucleotide encoded the T716M (A<u>C</u>G>A<u>T</u>G) substitution and a PAM-inactivating silent mutation in the T717 codon (AC<u>C</u>>AC<u>A</u>). For *Stat3^K658N^*, the sgRNA was produced based on a target site in exon 21 (CATG GATGCGACCAACATCC*TGG* = K658N, PAM italicised and underlined) of *Stat3*. The deoxy-oligonucleotide encoded the K658N (AA <u>G</u>>AA<u>C</u>) substitution and a PAM-inactivating silent mutation in the L666 codon (CT<u>G</u>>CT<u>C</u>).

For *Il10ra^KO^*, the sgRNA was produced based on a target site exon 3 (GGTGAA<u>C</u>GTTGTGAGATCAC*AGG*, PAM italicised and underlined) of *Il10ra*. The deoxy-oligonucleotide encoded the T86I (A<u>T</u>A>A<u>C</u>A) substitution and a PAM-inactivating silent mutation in the S82 codon (TCA>TC<u>C</u>). A founder carrying an 8bp frame shift mutation after the second base of the S82 codon was bred to establish the *Il10ra^KO^* line. For *Cx3cr1^KO^*, the sgRNA was produced based on a target site in the single coding exon, exon 2 (TACGCCCTCGTCTTCACGTT*CGG*, PAM italicised and underlined) of *Cx3cr1*. A founder mouse carrying an 1bp deletion that caused a frameshift after the T44 codon and an in-frame TGA stop signal 27 codons downstream was back-crossed with syngeneic partners to establish the *Cx3cr1^KO^* line. For *Klrk1^KO^*, the sgRNAs were produced based on target sites in intron 4 and the 3' UTR (TCA CAACGTGGTATAGTCCT*AGG* and GTTGAAGCCTATCCAAACTA*GGG*, PAM italicised and underlined) of *Klrk1*. A founder mouse that carried a 4,781 bp deletion in *Klrk1* that removed exons 4 to 8 (encoding the transmembrane and extracellular domains of NKG2D) was back-crossed with syngeneic partners and then inter-crossed to establish the *Klrk1^KO^* line.

C57BL/6 JAusb (C57BL/6J), C57BL/6 NCrl, B6.SJL-*Ptprc^a^Pepc^b^* (CD45.1) and B6.129S7-*Rag1^tm1Mom^*/J (*Rag1^KO/KO^*) mice were purchased from ABR.

Chimeras

Age- and sex-matched *Stat3^+/+^ Rag1^KO/KO^* C57BL/6J mice were irradiated with one dose of 425 Rad from an X-ray source (X-RAD 320 Biological Irradiator, PXI) and injected intravenously with 2–6 x 10^6^ lineage-depleted donor bone marrow from *Stat3^T716M^* or *Stat3^K658N^* WT or HOM mutant mice. The donor bone marrow was depleted of lineage-positive cells by MACS using a cocktail of antibodies to B220, CD3, CD4, CD8, CD11b, CD11c, CD19, LY-6C, LY-6G, NK1.1, TCRβ prior to injection. Recipients were sacrificed 8–14 weeks after transplantation to allow immune reconstitution.

Pathology phenotype scoring

Scores were calculated as equal weighted averages of severity scores on a scale from 0 to 3 (0 = undetectable; 1 = minor; 2 = moderate; 3 = major) for: (1) hair loss or inflammation around eyes, or cataracts; (2) skin inflammation on snout or face; (3) skin inflammation or 'flakiness' on ears; (4) skin inflammation or hair loss, primarily ventral, progressing to alopecia; (5) skin inflammation on tail, or ringtail.

In vivo monoclonal neutralising antibody treatments

Recipient *Stat3^K658N^* mice were mildly anesthetised by isoflurane and injected *i.p.* twice per week, to a total of 7 or 8 injections, with varying amounts of monoclonal antibodies as tabulated in the key resources table, and mice analyzed by flow cytometry 2–3 days after the last injection.

Isotype control antibodies were injected at equal concentration and final amount to the relevant treatment antibody.

Flow cytometry and cell-sorting

Peripheral blood mononuclear cells (PBMCs) were prepared from total blood collected from individuals with STAT3 GOF syndrome. In mice, single-cell suspensions were prepared from mouse spleen, bone marrow, inguinal lymph nodes, peritoneal cavity and blood. 1-4 x 10^6^ cells in PBS 2% FCS were transferred into appropriate wells of a 96-well U bottom plate. To prevent non-specific antibody binding, cells were incubated with F_c blocking antibody for 20 min at 4°C in the dark. Cells were then incubated with antibodies for 30 min, on ice and in the dark. To fix cells, they were incubated in 10% formalin (Sigma-Aldrich) for 15 min at 4°C, and washed and resuspended in PBS 2% FCS. To stain for intracellular nuclear proteins, cells were fixed and permeabilised using the manufacturer's instructions and the eBioscience Transcription Factor Staining kit. Stained single-cell suspensions were acquired on the BD LSRFortessa^TM^. Where appropriate, following extracellular antibody staining, immune populations were sorted by fluorescence-activated cell sorting (FACS) on a FACS Aria III (BD Biosciences).

Enzymatic digestion of mouse ears for flow cytometric analysis

At necropsy, ears were placed in PBS 2% FCS and cut into ~1mm pieces, resuspended in 600 μL RPMI with 1 μg/mL Collagenase (Sigma-Aldrich), 2 μg/mL Dispase II (Sigma-Aldrich) and 0.04U/1 μL DNase I (Sigma-Aldrich) and held 1 h in a rotating incubator at

37°C. The resulting cell suspensions were centrifuged at 500g for 4 min at 4°C, washed with 1000 μL PBS 2% FCS and passed through a 70 μM filter. The filtered suspension was centrifuged at 500g for 4 min at 4°C and the entire cell pellet was stained in PBS 1% FCS containing mAbs.

In vitro stimulation of splenic effector CD8+ T cells
Splenic naive and effector CD8+ T cells were FACS-purified based on TCRb, CD3, CD8, CD44 and CD62L expression. 10^4 cells were incubated per well for 3 days, in 200 μL of cRPMI alone, or cRPMI supplemented with (i) 5 μg/mL anti-CD3 (BioXCell; #145-2C11), (ii) 5 μg/mL anti-CD3 and 20 ng/mL recombinant mouse IL-15 (BioLegend; 566302), (iii) 1 ng/mL IL-15, (iv) 5 ng/mL IL-15 or (v) 20 ng/mL IL-15. Following 3 days of incubation, cells were analyzed for surface NKG2D expression by flow cytometry.

Single-cell RNA sequencing using the 10X platform
Human or mouse T cells were bulk sorted by FACS into Eppendorf tubes containing cold sterile PBS 10% FCS and incubated for 20 min at 4°C with TotalSeq™ DNA-barcoded anti-human or anti-mouse 'Hashing' antibodies (BioLegend) at a 1/100 final dilution. The TotalSeq-A™ antibodies conjugated to DNA oligonucleotides stained all leukocytes in the relevant samples. During the incubation, cells were transferred into a 96-well round bottom plate, on ice. Following incubation, cells were washed three times in cold PBS 2% FCS and the hashed populations pooled into mixtures for single-cell RNA sequencing using the 10X Genomics platform. In the case of human T cells, the hashed mixtures were first spiked with 3T3HEK mouse cells (2%) and incubated with DNA-barcoded antibodies (see key resources table), to allow high-throughput measurements of cell-surface proteins integrated with transcriptome measurements, by cellular indexing of transcriptomes and epitopes by sequencing (CITE-seq) (Stoeckius et al., 2017).

The Garvan-Weizmann Center for Cellular Genomics (GWCCG) performed the 10X capture, and sequencing of resulting cDNA samples, as an in-house commercial service, using the Chromium Single-Cell v2 3' Kits (10X Genomics) as per the manufacturer protocol. A total of 5,000 to 20,000 cells were captured per reaction.

RNA libraries were sequenced on an Illumina NovaSeq 6000 (NovaSeq Control Software v 1.6.0 / Real Time Analysis v3.4.4) using a NovaSeq S4 230 cycles kit (Illumina, 20447086) as follows: 28bp (Read 1), 91bp (Read 2) and 8bp (Index). HASHing libraries were sequenced on an Illumina NextSeq 500/550 (NextSeq Control Software v 2.2.0.4 / Real Time Analysis 2.4.11) using a NextSeq 60 cycles kit (Illumina, 20456719) as follows: 28bp (Read 1), 24bp (Read 2) and 8bp (Index). Sequencing generated raw data files in binary base call (BCL) format. These files were demultiplexed and converted to FASTQ using Illumina Conversion Software (bcl2fastq v2.19.0.316). Alignment, filtering, barcode counting and UMI counting were performed using the Cell Ranger Single Cell Software v3.1.0 (10X Genomics). Reads were aligned to the GRCh38 human (release 93) or mm10–3.0.0 (release 84) mouse reference genomes. Raw count matrices were exported and filtered using the EmptyDrops package in R (Lun et al., 2019).

Repertoire and gene expression by sequencing
The Repertoire and Gene Expression by Sequencing (RAGE-Seq) method (Singh et al., 2019) was applied in parallel, during 10X sequencing of T cells sorted from healthy controls or individuals with STAT3 GOF syndrome. Briefly, following full-length cDNA 10X capture generation, the cDNA library was split into two prior to fragmentation for short-read sequencing. In parallel to the standard 10X Illumina library preparation and short-read sequencing, full-length sequencing was performed using Oxford Nanopore on selectively-enriched BCR and TCR cDNA transcripts obtained by targeted hybridisation capture, to obtain both the 3' cell-barcode and the 5' V(D)J sequence. Cell barcodes were then matched between short-read sequencing and antigen-receptor sequences.

TCR deep sequencing by modified 5'RACE
RNA was extracted from T cell populations bulk-sorted by FACS, using the Qiagen AllPrep DNA/RNA Mini Kit (#80204). cDNA synthesis was performed on 2.5 μL of RNA using the cDNA synthesis and library amplification method from the Smart-Seq2 protocol (Picelli et al., 2014). 10 cycles of PCR amplification were performed and the TSO oligo was modified to incorporate a 10 bp unique molecular identified (UMI). Following purification of PCR products with magnetic AMPure XP beads (Agencourt), TCRβ-specific PCR was performed with a primer targeting the constant region of the TCRβ chain and a forward primer (ADP_fwd) targeting the 5' incorporated TSO oligo.

PCR **was** performed using the KAPA HiFi HotStart Ready Mix (Kappa Biosystems), under the following conditions: 98°C 45s; 30 cycles: 98°C 15s, 60°C 30s, 72°C 30s; 72°C 1min. The PCR products were purified using AMPure beads and complete adaptor sequences and sample barcodes were added using the primers from the Illumina Nextera Index Kit (Illumina).

5 cycles of PCR amplification were performed using the Q5 High-Fidelity DNA Polymerase kit (New England BioLabs): 72 3min; 98°C 30s; 5 cycles: 98°C 10s, 63°C 30s, 70°C 3min. Following a second round of magnetic bead purification, the TCR libraries were quantified using the Qubit 4 fluorometer (Invitrogen) and pooled at equal concentration for sequencing on an Illumina MiSeq 250 bp paired-end run.

Sequencing was performed on the Illumina MiSeq platform using the MiSeq Reagent Kit v3 with a read length mode of 2 x 300bp. Libraries were sequenced to ~1 million reads per sample.

QUANTIFICATION AND STATISTICAL ANALYSIS

Following flow cytometric experiments, statistical analyses were performed using the GraphPad Prism 6 software (GraphPad, San Diego, USA). A one-tailed unpaired Student's *t* test with Welch's correction was used for comparisons between two normally

distributed groups. An unpaired Student's *t* test, corrected for multiple comparisons using the Holm-Sidak method, was used for comparisons of more than two groups. Differences between paired measurements were analyzed by paired t-test. In all graphs presented, the error bars represent the mean and standard deviation. $*p < 0.05$, $**p < 0.01$, $***p < 0.001$.

Following TCR deep sequencing, sequencing libraries were de-multiplexed by their sample indices using the Illumina FASTQ generation workflow. Paired-end reads were merged using FLASH (Magoc and Salzberg, 2011). Quality filtering, UMI extraction, primer trimming and de-replication were performed using pRESTO (Vander Heiden et al., 2014). The resulting FASTA formatted sequence datasets were aligned against the germline reference directory for the locus and species obtained from IMGT [http://www.imgt.org/] using a local installation of IgBLAST (Ye et al., 2013). IgBLAST alignment determined the V, D and J gene segments that contributed to each rearrangement, any nucleotide insertions or deletions when the segments were joined, the FR and CDRs. TCR repertoires were summarised at the clonotype level, with clonotypes defined as sequences that shared the same V gene, J gene and CDR3 AA sequence.

For nanopore sequencing, RAGE-seq contigs for each cell barcode were generated and TRA and TRB chains for each cell were assigned as described in (Singh et al., 2019). Clonotypes from RAGE-seq were defined and summarised using the same approach as for the repertoire sequencing.

For the 10X analysis of mouse CD8$^+$ T cell populations, cells were excluded if the library size or number of expressed genes fell below 2 median absolute deviations, or if mitochondrial reads accounted for more than 20% of total reads. Cell-wise gene expression counts were normalized and recovered using SAVER (Huang et al., 2018) with default values, and differentially expressed genes (DEGs) were identified using limma (Ritchie et al., 2015) on the log-transformed recovered counts. Bonferroni correction was applied to each set of *p-value*s. DEGs were defined as having a family-wise error rate (FWER) < 0.05.

For the 10X analysis of human T cell populations, raw BCL files were demultiplexed and aligned to human genome reference GRCh38 and mouse genome reference mm10, using CellRanger v3.0.2 (10X Genomics) to generate UMI count matrices. CellRanger "filtered_barcode" count matrices were processed by removal of any barcodes with less than 100 genes or 1000 UMI's or with more than 25% mitochondrial content. All cells with between 5 and 95% mouse UMI's were classified as having high ambient mRNA (defined as mRNA molecules not present inside a cell before/at time of capture) and therefore removed. R package Seurat (Satija et al., 2015) v3.0.4 was used for normalisation, dimensionality reduction and cluster assignment using default parameters (at resolution 0.8), using all principal components (n = 100) found to be significant ($p \leq 0.01$) as calculated by the Seurat function Jackstraw. Having first benchmarked batch correction and integration using Harmony and Seurat v3 compared to the SCTransform workflow, we proceeded using the Harmony workflow with default settings. We provided the Harmony Matrix function with all n = 100 PCAs found to be significant by Jackstraw. Samples were batch-corrected and integrated using R package Harmony v.1.0 using the same statistically significant principal components.

For the CITE-seq analysis of human T cell populations, FASTQ reads were demultiplexed and aligned to the ADT barcode library using package CITE-seq count v1.4.3 (https://github.com/Hoohm/CITE-seq-Count), using the barcode 'whitelist': barcodes meeting quality control requirements following CellRanger v3.0.2 "filter barcode". UMIs were collapsed using a maximum hamming distance error of 1 for both cell barcode and UMI. The processed ADT UMI count matrices were normalised and scaled using Seurat v3.0.4 default parameters, as per the developer's protocol for CITE-seq (Stoeckius et al., 2017).